Real-time UV-Index retrieval in Europe using Earth Observation based techniques and validation against ground-based measurements

Panagiotis G. Kosmopoulos[1], Stelios Kazadzis[2], Alois W. Schmalwieser[3], Panagiotis I. Raptis[1], Kyriakoula Papachristopoulou[1], Ilias Fountoulakis[1,4], Akriti Masoom[5], Alkiviadis F. Bais[6], Julia Bilbao[7], Mario Blumthaler[8], Axel Kreuter[8,9], Anna Maria Siani[10], Kostas Eleftheratos[11], Chrysanthi Topaloglou[65], Julian Gröbner[2], Bjørn Johnsen[12], Tove Svendby[13], Jose Manuel Vilaplana[14], Lionel Doppler[15], Ann R. Webb[16], Marina Khazova[17], Hugo De Backer[18], Anu Heikkilä[19], Kaisa Lakkala[20], Janusz Jaroslawski[21], Charikleia Meleti[5], Henri Diémoz[4], Gregor Hülsen[2], Barbara Klotz[8], John Rimmer[16], Charalampos Kontoes[1]

[1]National Observatory of Athens, Athens, Greece
[2]Physikalisch-Meteorologisches Observatorium Davos, World Radiation Center, Davos Dorf, Switzerland
[3]University of Veterinary Medicine, Vienna, Austria
[4]Environmental Protection Agency of Aosta Valley, Aosta, Italy
[5]Indian Institute of Technology Roorkee, India
[6]Aristotle University of Thessaloniki, Greece
[7]Valladolid University, Valladolid, Spain
[8]Innsbruck Medical University, Innsbruck, Austria
[9] Luftblick OG, Innsbruck, Austria
[10]Sapienza University of Rome, Rome, Italy
[11]National and Kapodistrian University of Athens, Athens, Greece
[12]Norwegian Radiation and Nuclear Safety Authority, Bærum, Norway
[13]Norwegian Institute for Air Research, Bærum, Norway
[14]National Institute for Aerospace Technology, Torrejón de Ardoz, Spain
[15]German Weather Service, Offenbach, Germany
[16]University of Manchester, Manchester, UK
[17]Public Health England, London, UK
[18]Royal Meteorological Institute of Belgium, Bruxelles, Belgium
[19]Finnish Meteorological Institute, Helsinki, Finland
[20]Finnish Meteorological Institute, Sodankylä, Finland
[21]Institute of Geophysics, Polish Academy of Sciences, Warsaw, Poland

Correspondence to: P.G. Kosmopoulos (pkosmo@noa.gr)

Abstract. This study introduces an Earth observation (EO)-based system which is capable of operationally estimating and continuously monitoring the ultraviolet index (UVI) in Europe. The UVIOS (i.e. UV-Index Operating System) exploits a synergy of radiative transfer models with high performance computing and EO data from satellites (Meteosat Second Generation and Meteorological Operational Satellite-B), and retrieval processes (Tropospheric Emission Monitoring Internet Service, Copernicus Atmosphere Monitoring Service and the Global Land Service). It provides a near-real-time now-casting

and short-term forecasting service for UV radiation over Europe. The main atmospheric inputs for the UVI simulations include ozone, clouds and aerosols while the impacts of ground elevation and surface albedo are also taken into account. The UVIOS output is the UVI at high spatial and temporal resolution (5 km and 15 minutes, respectively) for Europe (i.e. 1.5 million pixels) in real-time. The UVI is empirically related to biologically important UV dose rates and the reliability of this EO-based solution was verified against ground-based measurements from 17 stations across Europe. Stations are equipped with spectral, broadband or multi-filter instruments and cover a range of topographic and atmospheric conditions. A period of over one year of forecasted 15-min retrievals under all sky conditions were compared with the ground–based measurements. UVIOS forecasts were within ±0.5 of measured UVI for at least 70% of the data compared at all stations. For clear sky conditions the agreement was better than 0.5 UVI for 80% of the data. A sensitivity analysis of EO inputs and UVIOS outputs was performed in order to quantify the level of uncertainty in the derived products, and to identify the covariance between the accuracy of the output and the spatial and temporal resolution, and the quality of the inputs. Overall, UVIOS slightly overestimated UVI due to observational uncertainties in inputs of cloud and aerosol. This service will hopefully contribute to EO capabilities and will assist the provision of operational early warning systems that will help raise awareness among European Union citizens of the health implications of high UVI doses.

Keywords. Ultraviolet Index; Earth Observation; Radiative Transfer; High Performance Computing; Clouds; Aerosols; Ozone; Solar Zenith Angle; Ground Elevation; Surface Albedo

1 Introduction

Human exposure to ultraviolet (UV) radiation has both beneficial and harmful effects (Andrady et al., 2015; Juzeniene et al., 2011; Lucas et al., 2006). Overexposure to UV radiation (UVR) has a number of implications, such as the acute response of erythema, the risk of skin cancer and a number of eye diseases (snow blindness, cataract). Nevertheless, exposure to solar UVB radiation is the main mechanism for the synthesis of Vitamin D in the human skin (Holick, 2002; Webb and Engelsen, 2008; Webb et al., 2011). Low levels of the Vitamin D are associated with depression of the immune system and there is evidence that is linked to a number of medical implications (Lucas et al., 2015).

The UV index was introduced by WHO/WMO in 1994 (WMO, 1995), as a simple method of informing the general public about the erythema effective (sun-burning) UV. It is a unitless, scaled version of erythemally-weighted UV determined by multiplying the erythema weighted irradiance (in W/m^2) by 40 m^2/W (Fioletov et al., 2010 ; Vanicek et al., 2000; WHO, 2002). The response of UV radiation to climatic changes is of great concern (Bais et al., 2019; Bais et al., 2018; McKenzie et al., 2011). According to the latest work of Bais et al. (2019) greater values of UV are expected by the end of 21st century, relative to the present decade, at low latitudes, while at higher latitudes UV will decrease but these projections are associated with high uncertainty (up to 30%).

69 There are many factors affecting UV irradiance reaching Earth's surface (Kerr and Fioletov, 2008). The dependence of UV

70 irradiance on astronomical and geometrical parameters is generally well understood, and in many cases the changes are

71 periodical (e.g., (Blumthaler et al., 1997; Gröbner et al., 2017; Larkin et al., 2000; Seckmeyer et al., 2008)). Atmospheric gases

72 play a crucial role in attenuating UV irradiance, ~~with~~specifically NO_2 is a major absorber in this spectral region (e.g., Cede et

73 al. (2006)), while O_3 ~~being~~is the main absorber at lower (UVB) wavelengths~~in the UVB (Bais et al., 1993), and NO₂ being the~~

74 ~~main absorber in the UV-A (e.g. Cede et al. (2006)) spectral region~~. Other gases that have significant absorption in the UV

75 include SO2 (Fioletov et al., 1998) and HCHO (Gratien et al., 2007), but their –usually- smaller atmospheric abundances,

76 result in minor effects to incoming UV (with major exceptions such as volcanic incidents). Aerosols are another important

77 parameter controlling UV irradiance levels at the surface (e.g., Kazadzis et al. (2009b)). Aerosol optical depth (AOD) that

78 quantifies the attenuation of the direct solar beam by aerosols is a parameter varying with wavelength, as well as single

79 scattering albedo (SSA), which determines the scattering ratio to total extinction. Several recent studies based on incoming

80 UV irradiance measurements or calculations reveal the enhanced absorption by aerosols in the UV relative to the visible

81 spectral range. They show the importance of using SSA in the UV spectral region, instead of interpolating SSA at visible

82 wavelengths to the UV, or directly using SSA at visible wavelengths, options that systematically overestimate UV irradiance

83 (Corr et al., 2009; Fountoulakis et al., 2019; Kazadzis et al., 2016; Mok et al., 2018; Raptis et al., 2018).

84 All the aforementioned parameters are particularly important under cloud free conditions. The cloudy sky complicates the

85 propagation of solar radiation, predominantly in the troposphere, through multiple cloud - radiation interactions. Nonetheless,

86 UVR is less affected than the total solar radiation by clouds (e.g., Badosa et al. (2014)). Bais et al. (1993) quantified that for

87 the city of Thessaloniki the change from 0 to ~~8/~~8 oktas for cloud coverage corresponds to 80% reduction in the UVR and

88 pointed out that there is very low wavelength dependence of UVR attenuation by cloud cover. Although, the transmittance of

89 clouds does not vary significantly with wavelength, some ~~In other~~ studies (Mayer et al., 1998; Seckmeyer et al., 1996) have

90 found that the diffuse component of the surface UVR is affected by clouds in a spectrally dependent way, due to more efficient

91 scattering and absorption of shorter UV wavelengths, in case of large air masses~~the authors showed that although the~~

92 ~~transmittance of clouds does not vary significantly with wavelength in the UV, clouds give a wavelength dependent effect to~~

93 ~~the diffuse component the surface UVR, due to the more effective scattering and absorption of shorter UV wavelengths in the~~

94 ~~atmosphere acting on larger air masses~~. In cases of partially cloudy sky but unobscured sun, UVR tends to be higher than in

95 clear sky conditions (e.g., Badosa et al. (2014)), as is the case for total solar radiation. For short timescale analysis the

96 variability of UVR introduced by clouds should be considered. ~~A review of empirical studies of cloud effects on UVR is given~~

97 ~~by Calbó et al. (2005).~~

98 Solar UV irradiance at the surface increases with increasing surface albedo. This increment affects the UV radiant exposure,

99 which becomes crucial for outdoor human activities (Schmalwieser and Siani, 2018; Schmalwieser, 2020; Siani et al., 2008).

100 Measurements and computations of effective surface albedo for heterogeneous surfaces reveal its strong spectral dependence,

101 with snow-covered surfaces having significantly higher values of albedo for short wavelengths compared to total solar radiation

(Blumthaler and Ambach, 1988; Kreuter et al., 2014). Stronger enhancement of the UV relative to visible radiation over highly reflective surfaces is also due to the more effective multiple scattering of shorter wavelengths in the atmosphere.

Any systematic changes in any of the parameters described in previous paragraphs have the potential to lead to changes for UVR. These changes vary significantly throughout the globe and are attributed to different possible drivers (Bernhard and Stierle, 2020; Fountoulakis et al., 2018; McKenzie et al., 2019). Fountoulakis et al. (2020a) gives a review of recent publications concerning UV trends since 1990s, and associated factors, summarizing these as positive trends for South and Central Europe and negative trends at higher latitudes, and recognizing the important role of aerosols and cloud coverage for these trends in contrast to ozone. Findings from the same study demonstrated that the long – term changes of UV irradiance recorded at four stations around Europe during the last two decades are mainly attributed to aerosols, cloud coverage and surface albedo variations, with total ozone changes being of minor importance.

Chubarova et al. (2020) found a long term increase of 3% per decade in UV at Northern Eurasia for the 1979-2015 period. For the northern mid-latitudes Zerefos et al. (2012) showed that the long-term (1995-2006) positive trends in total ozone wasn't enough to compensate for, let alone reverse, the UVB increase attributed to tropospheric aerosol decline (brightening effect). Since 2007, a slowdown or even a possible turning point in the positive UVB trend was detected, which was attributed to the continued upward trend in total ozone overwhelming the aerosol effect (Zerefos et al., 2012. By contrast, the long-term variability of UVB irradiance over northern high latitudes was determined by ozone and not by aerosol trends, as shown by Eleftheratos et al. (2015) who found a statistically significant negative trend of -3.9% per decade for the UVB irradiance during the time period 1999-2011, from gGround-bBased (GB) measurements at 7 stations. This was in agreement with statistically significant increase of spaceborne measured total ozone by about 1.5% per decade (ozone recovery) for the same area. For Arctic regions changes in snow cover have a great impact on UV trends according to Bernhard (2011), who concluded that the future Arctic UV climate may be affected more by a warming climate changing the snow cover than changes in stratospheric ozone concentrations.

The continuous monitoring of the UV index is currently performed by about 160 stations from 25 countries around Europe (Schmalwieser et al., 2017), with all monitoring instruments having the potential to provide other effective doses such as the effective dose for the production of vitamin D in human skin (e.g., Fioletov et al. (2009)).

There are three types of instruments for UV irradiance measurements; those measuring the integral of UV irradiance (broadband sensors) tailored to a specific response, narrow band instruments such as filter radiometers with coarse spectral resolution, and instruments performing high resolution spectral measurements – the most versatile but most challenging and least robust instruments. Concerning the current UV monitoring measurement accuracy; The European reference UV spectroradiometer (QASUME) is a traveling instrument which provides a common standard through inter-comparison on-site (Gröbner et al., 2005; Hülsen et al., 2016). During the period 2000-2005 the QASUME visited 27 spectroradiometers sites. Out of the 27 instruments, 13 showed deviations of less than 4% relative to the QASUME reference spectroradiometer in the UVB (for 15 instruments in the UVA) for solar zenith angles below 75°. The expanded relative uncertainty (coverage factor k=2) of solar UV irradiance measurements by QASUME, for SZA smaller than 75° and wavelengths longer than 310 nm, was

136   4.6% in 2002 – 2014 (Gröbner and Sperfeld, 2005), and has been 2 % since 2014 (Hülsen et al., 2016). For broadband

137   instruments, the current instrument uncertainties are summarized in (Hülsen et al., 2020; Hülsen et al., 2008). In 2017, 75

138   broad-band instruments measuring the UV index, the UVB or/and the UVA irradiance participated in the solar UV broadband

139   radiometer comparison in Davos Switzerland. Using the instrument/user calibration factors, the differences between the

140   datasets by the broad-band instruments and the reference (QASUME) dataset were within ±5 % for 32 (43 %) of the instrument

141   datasets, ±10 % for 48 (64 %), and exceeded ±10 for % 27 (35 %).

142   Although ground-based monitoring of solar UVR is more accurate than satellite retrievals, ground based stations are sparse,

143   and the only way for continuous monitoring of the UVR on a global scale is through satellites. In recent decades instruments

144   on-board satellites have provided the necessary data for estimates of UV irradiance reaching the Earth surface on a global scale

145   (Herman, 2010) and hence satellite-derived UVR climatological studies have been conducted (Vitt et al., 2020; Verdebout,

146   2004). The satellite UV irradiance record started with the Total Ozone Mapping Spectrometer (TOMS) on-board Nimbus-7 in

147   1978 and continued with Ozone Monitoring Instrument (OMI) on-board NASA's satellite EOS-Aura. The OMI retrieval

148   algorithm for surface UVR estimates was based on the experience gained from TOMS (Levelt et al., 2018; Levelt et al., 2006).

149   The early surface UVR retrieval algorithms from satellite data didn't account for the enhanced aerosol absorption in the UV

150   spectral range, resulting in overestimated values (Krotkov et al., 1998). A lot of scientific effort has been put into correcting

151   the products (Arola et al., 2009). TROPOspheric Monitoring Instrument (TROPOMI) onboard Sentinel – 5 Precursor (Lindfors

152   et al., 2018) is the current satellite instrument that provides the surface UVR product on a daily basis with global coverage,

153   including 36 UVR parameters. As the aforementioned instruments were installed onboard polar orbitting satellites, providing

154   global spatial coverage, the temporal resolution of the data is daily since there are only one or two overpasses per day for every

155   point. Geostationary satellites provide continuous (in time) measurements over wide areas. The geostationary meteorological

156   satellites Meteosat monitor the full Earth Disk including Europe and their frequent data acquisition of rapidly changing

157   parameters e.g., cloud is essential for estimating daily UV doses (e.g. Verdebout, 2000 Verdebout (2004)). Comparison of OMI

158   surface UV irradiance estimates with ground-based measurements for Thessaloniki, Greece showed that OMI irradiances

159   overestimate surface observations for UVB wavelengths by between ~1.5% to 13.5% in contrast to underestimated satellite

160   values for UVA wavelengths (Zempila et al., 2016). Results from the validation of TROPOMI surface UV radiation product

161   showed that most of the satellite data agreed within ± 10 % with ground-based measurements for snow-free surfaces (Lakkala

162   et al., 2020). Larger differences between satellite data and ground-based measurements were observed for sites with non-

163   homogeneous topography and non-homogeneous surface albedo conditions. The differences between ground-basedGB and

164   satellite UVR data are mostly due to uncertainties in the input parameters to the satellite algorithm used to retrieve the UV

165   irradiance at the surface. Based on a recent study of Garane et al. (2019) a mean bias of 0-1.5% and a mean standard deviation

166   of 2.5 – 4.5 % was found for the relative difference between TROPOMI total ozone column (TOC) product and ground based

167   quality assured Brewer and Dobson TOC measurements.

168   In this study we introduce present a novel UV-Index Operating System, called UVIOS, which is able to efficiently combine

169   information on geophysical input parameters from different modelled and satellite-based data sources in order to provide

170 ~~nowcast and forecast~~ for the European region the best possible UV-Index (UVI) estimates operationally and in real-time.

171 UVIOS~~by using~~ is based on pre-calculated radiative transfer model simulations in the form of analytical look-up tables (LUT)

172 in conjunction with ~~atmospheric~~ geophysical input parameters ~~from satellites~~ and high performance computing for

173 instantaneous outputs ~~of the order of 20 million grid points in less than 1 minute.~~ ~~The Earth-Observation-based atmospheric~~

174 ~~inputs were retrieved operationally for the year 2017 and include the effects of aerosols, clouds, solar and ground elevation,~~

175 ~~surface albedo and ozone. The aforementioned computing architecture formed a novel system called UVIOS (i.e. UV Index~~

176 ~~Operating System).~~ The reliability of the UVIOS input and output parameters was tested for the year 2017 against ground-

177 based measurements and an analytical sensitivity analysis was performed in order to quantify the uncertainties and to provide

178 information about the limitations and about the optimum operating conditions of the proposed system~~methodology~~. Since

179 UVIOS can produce massive UVI outputs of the order of 1.5 million simulations in less than 5 minutes following the proposed

180 simulation and computing architecture (see section 2.1.2), this means that it can be used for both operational applications and

181 real-time estimations. The exact use of UVIOS depends only on the available input data sources. For this study both nowcasts

182 (clouds) and forecasts (ozone, aerosol) were used as inputs to the system. The nowcasts represent the continuous monitoring

183 dimension (i.e. what is happening now) in terms of cloud microphysics data every 15 minutes retrieved in real-time by the

184 geostationary satellite Meteosat Second Generation (MSG). The forecasts represent the future estimations (day ahead in our

185 study) of aerosol optical properties and total ozone column based on deterministic approaches (ECMWF) and assimilated

186 satellite data for better accuracy. As a result, UVIOS under cloudless conditions operates as a forecast system since it uses

187 forecasted inputs and provides the clear-sky UVI forecasts operationally. By adding the nowcast cloud information as input to

188 UVIOS (i.e. all sky conditions), the whole procedure will follow the time steps of MSG cloud microphysics data collocated

189 and synchronized with the forecast data. So, following the proposed operation method of this study, the UVIOS can be used

190 as a UVI forecast system for cloudless conditions or as a UVI nowcast system for all sky conditions.

191 In Section 2 we describe the UVIOS, the input data sources and the ground-based measurements used for the validation.

192 Section 3 presents the results in terms of model performance and factors that affect the UVIOS retrievals and the overall

193 accuracy. Finally, Section 4 summarizes the findings and the main conclusions of this study.

2 Data and Methodology

2.1 The UV Index operating system (UVIOS)

2.1.1 UVIOS modelling

197 The UVIOS system is a novel model that uses real-time and forecasted atmospheric inputs based on satellite retrievals and

198 modelling techniques and databases in order to nowcast and forecast the UVI with a spatial resolution of 5 km and a temporal

199 resolution of 15 minutes. The UVIOS calculation scheme is based on the libRadtran library of radiative transfer models (RTM)

(Mayer and Kylling, 2005) within which all the available inputs (i.e. solar elevation, cloud and aerosol optical properties, ozone) can be integrated in real-time into the radiative transfer code and calculate the UVI for each pixel. Afterwards, post processing correction for the elevation of each location and the surface albedo is also performed. In order to be able to simulate the UVI for 1.5 million pixels in real-time we use pre-determined spectral solar irradiance LUTs based on the Librdtran RTM, in combination with high performance computing (HPC) architectures that speed up the process of choosing and interpolating/extrapolating the right combinations from the LUTs (Kosmopoulos et al., 2018; Taylor et al., 2016). The result is the retrieval of UVI for 1.5 million pixels covering the European domain in less than 5 minutes after receiving all necessary input parameters.

As mentioned the UVIOS architecture does not include a clear sky model and the subsequent calculation of individual sources of UV attenuation, but instead it directly uses the following parameters: solar zenith angle (SZA), the aerosol optical depth (AOD) and other aerosol optical properties (e.g., single scattering albedo (SSA), asymmetry parameter, and Ångström exponent (AE)), the total ozone column (TOC), the cloud optical thickness (COT), as well as the surface elevation (ELE) and the surface albedo (ALB) as RTM inputs. Table 1 presents the EO data used as inputs for the UVI real time simulations, their description and sources. The Meteosat Second Generation (MSG4) cloud microphysics includes the nowcasted cloud optical thickness (COT) at 550 nm, and cloud phase (CPH) obtained at a spatial and temporal resolutions of 5 km (average, depending on latitude) and 15 minutes, respectively. Typical values of other cloud properties (e.g., cloud height, cloud thickness) have been assumed based on the cloud type (information which is also available from MSG) (for more detailed information see Taylor et al. (2016). The 1-day forecast CAMS aerosol optical depth (AOD) at 550 nm is obtained at a spatial and temporal resolutions of 40 km and 3 h, respectively and the monthly aerosol optical properties obtained from Aerocom (Kinne, 2019) includes asymmetry parameter, single scattering albedo (SSA) and Ångström exponent (AE) at 1º x 1º (latitude x longitude) spatial resolution. Solar elevation is taken from the Astronomical model (NREL) (5 km – 15 minutes) (Reda and Andreas, 2008) and climatological surface albedo (ALB) is retrieved from Copernicus Global Land Service (CGLS) (1 km – 12 days) (Carrer et al., 2010). Surface elevation (ELE) is obtained from the Digital Elevation Model (DEM) of NOAA (NOAA, 1988). The Tropospheric Emission Monitoring Internet Service (TEMIS) 1-day forecast of total ozone column (TOC) is at a spatial resolution of 1º x 1º – 1 day with assimilated ozone fields from GOME-2 (METOP-B) (Eskes et al., 2003). We have to mention also here that the selection of the RTM inputs has been decided based on their real-time availability.

2.1.2 UVIOS real-time processing concept

The LUT approach, despite its large size (almost 2.5 million spectral RTM simulations for clear and all sky conditions) (Kosmopoulos et al., 2018), still provides estimates at discrete input parameters values. To overcome this mathematical issue, we performed a multi-parametric interpolation technique to correct the input-output parameter intervals. This solution is computationally more costly than a continuous function-approximation model, i.e. a Neural Network (NN) model (Kosmopoulos et al., 2018), but the accuracy improvement is significant. Indicatively, using a test set of 1 million RTM

232 simulations for UVI from the developed LUT, we applied the NN developed in Kosmopoulos et al. (2018) and found a mean

233 execution time of around 144 seconds followed by a mean absolute error (MAE) of 0.0321, while by using the proposed

234 UVIOS multi-parametric interpolation exploiting the HPC and distributed computing benefits we found for the same test set

235 an execution time of 295 seconds with a MAE of 0.0001. The inclusion of many parameters (in this study we incorporated

236 eight, i.e. AOD, SZA, TOC, COT, ELE, ALB, AE, SSA) with small step sizes dramatically increase the LUT size, followed

237 by high computing requirements for the multi-parametric interpolation/extrapolation procedures.

238 For the UVIOS simulations performed in this study, a 32-core UNIX server was used equipped with 256 Gb of RAM and 12

239 Tb of storage system working in a RAID10 architecture. The combination of the HPC with the analytical LUTs, which were

240 developed by using the libRadtran RTM, allow a high speed multi-parametric interpolation and polynomial reconstruction

241 (Gal, 1986) to increase accuracy between the LUT records following a mathematical equation relating the UVIOS outputs to

242 the EO inputs.

243 An example of the UVIOS input output data is presented in Figure 1 through a flowchart illustration of the modelling technique

244 scheme. The inputs, including the solar and surface elevation, albedo, aerosol, ozone forecasts and the cloud observations as

245 described in Table 1, are fed to the real-time solver that results in spectrally weighted output of UVI for the European region.

246 Figure 2 shows the memory usage and error statistics for a range of different LUT sizes. The LUT error decreases as the LUT

247 size increases, regardless of the function being approximated. The LUT sizes in Figure 2 fit into cache on our HPC

248 environment, thus performance in terms of processing speed and overall output accuracy vary only slightly between the table

249 sizes shown. In our case, UVIOS shows that LUT transformation can provide a significant performance increase without

250 incurring an unreasonable amount of error, provided there is sufficient memory available. We note that the cache size is a

251 critical factor for LUT performance, while under a HPC environment practically there is no limit. Such techniques can be

252 implemented in hardware with distributed computing that operates in parallel to provide optimum performance.

253

254 **2.2 ~~Earth Observations~~The description of the geophysical parameters**

255 The Cloud Optical Thickness (COT) data from Meteosat was used, whose retrieval algorithm is based on 0.6 and 1.6 micron

256 channel radiances of Meteosat's Spinning Enhanced Visible and InfraRed Imager (SEVIRI). MSG products have been

257 described in Derrien and Le Gléau (2005) and the MétéoFrance (2013) technical report. The COT impact uncertainty on UVI

258 deals with the MSG COT reliability and accuracy and hence introduces errors into the UVIOS simulations (Derrien and Le

259 Gléau, 2005; Pfeifroth et al., 2016). In addition, comparison principles of (point) station UVI measurements with a 5 km MSG

260 COT matrix are possibly responsible for at least part of the observed deviations (e.g., Kazadzis et al. (2009a)). For instance,

261 when a MSG pixel is partly cloudy, the ground measurements of UVI could fluctuate more than 100%, depending on whether

262 the sun is visible or whether clouds attenuate the direct component of the solar irradiance. The result is that in cases of partly

263 covered MSG pixels and in the absence of clouds between the ground measurement and the sun, the ground truth UVI would

be much higher than the UVIOS one. Of course, the presence of small clouds which have not been identified by MSG and cover (part of) the sun disk, is plausible as well, consequently causing an overestimation of the modelled UVI (Koren et al., 2007). Furthermore, sensors onboard geostationary satellites suffer from the parallax error, which contributes to the spatial errors of the images and the overall uncertainty of the products (Bieliński, 2020; Henken et al., 2011). The error depends on the altitude of the cloud and the viewing angle (parallax errors are more significant for high viewing angles).

UVIOS calculations at high solar zenith angles (>70̶5̶ deg) are retrieved assuming cloudless skies since the MSG COT product is not available in these conditions, facing reliability issues (Kato and Marshak, 2009). This has an effect on the quality of the UVIOS overall performance at high solar zenith angles, where there is no cloud information as input to the model in order to quantify the consequent impact on UVI. However, ̶s̶i̶n̶c̶e̶ such measurements under high solar zenith angles are ̶a̶s̶s̶o̶c̶i̶a̶t̶e̶d̶accompanied with very low UV-̶I̶n̶d̶e̶x̶ levels (<1) both in the performed RTM simulations and in the ground-based measurements.̶,̶ ̶T̶this inconsistency, even if does not affect UVIOS UV-̶I̶n̶d̶e̶x̶ results associated with dangerous effects on human health, nevertheless it is still affected by the rest of input parameters (i.e. ozone, aerosol etc) mitigating the UVIOS uncertainty in the absence of cloud information under such high solar zenith angles. There is more discussion in the next section on how we use these data for the UVIOS validation.

For the total aerosol optical depth, we used 1-day forecast data from the Copernicus Atmospheric Monitoring Service (CAMS) as the basic input parameter. These forecasts are based on the Monitoring Atmospheric Composition and Climate (MACC) analysis and provide accurate data of aerosol optical depth (AOD) at 550 nm with a time step of 1 h and spatial resolution of 0.4°.

For aerosol single scattering albedo properties climatological values from MACv2 aerosol climatology (Kinne, 2019) was utilized. Monthly means of single scattering albedo at 310nm were acquired from global gridded data at a 1° x 1° spatial resolution. Also, in order to derive the Angstrom exponent, monthly means of AOD at 340nm and 550nm were used. The calculated Ångström exponent was then applied to the 550 nm AOD (from CAMS) in order to get AOD in the UV.

The surface albedo data were obtained from the Copernicus global land service (CGLS: Geiger et al., 2008; Carrer et al., 2010). As a global surface ALB product is not available in the UV region, for this study we have used the climatological product of CGLS (in the visible range) (Lacaze et al., 2013) as follows: based on the findings of Feister and Grewe̶,̶ (1995)̶;̶:̶ we used a UV albedo of 0.05 for non-snow cases and a UV ALB equal with CGLS when CGLS exceeded 0.5 (snow cover). The total ozone column forecasts were obtained from Tropospheric Emission Monitoring Internet Service (TEMIS) which is a near- real time service which uses the satellite observations of total ozone column by the Global Ozone Monitoring Experiment (GOME) and SCIAMACHY assimilated in a transport model, driven by the European Centre for Medium-Range Weather Forecasts (ECMWF) forecast meteorological fields (Eskes et al., 2003). The elevation data was obtained from the 5-minute Gridded Global Relief Data (ETOPO5) database, which provides land and seafloor elevation information at a 5-minute latitude/longitude grid, with a 1-meter precision in the region of Europe and is freely available from NOAA (NOAA, 1988). An analytical description of the above geophysical parameters including their specifications and resolution can be found in Table 1, followed by the corresponding references for more technical details. Figure 3 shows an example of the input-output

UVIOS parameters. An extensive validation of the MACC analysis and forecasting system products were performed by Eskes et al. (2015). The aerosol optical properties were validated against 3-year (Apr. 2011 – Aug. 2014) near real time level 1.5 AERONETeronet measurements and for AOD at 550 nm an overall overestimation was exhibited. Due to dedicated validation activity of the MACC service a validation report that covers the time period of this study (Eskes et al., 2018) is also available, presenting an overall positive modified normalized mean bias during 2017, ranging from 0 to 0.4, with the same range of values over the study region (Europe). This overestimation of AOD at 550 nm may explain some of the UVI underestimation under clear sky conditions (see section 3.2.2).

2.3 Ground-based measurements

In order to validate the UVIOS results 17 ground based stations were selected, for which measurements of the UVI were available during 2017. The stations are shown in Fig. 4. Comparisons were performed with a 15-minute step. The ground based measurements were obtained from spectrophotometers (Brewer), spectroradiometers (Bentham), filter radiometers (GUV) and broadband instruments (SL501 and YES) as Table 2 shows. INote that UV data in table 2 has been calibrated, processed and provided directly by the responsible scientists for each station. References wherein more information for the data quality of particular instruments can be found are also provided. Brewer spectrophotometers measure the global spectral UV irradiance with a step of 0.5 nm, and a resolution which is approximately 0.5 nm (usually between 0.4 and 0.6 nm). Depending on their type the spectral range is usually 290-325 nm (MKII, MKIV) or 290-363 nm (MKIII,). Since Brewer spectrophotometers measure the spectrum up to a wavelength which is shorter than 400 nm, extension of the spectrum up to 400 nm in order to calculate the UV index is usually achieved using empirical methods (e.g., (Fioletov et al., 2003; Slaper et al., 1995)). The additional uncertainty in the UVI due to the latter approximation is well below the overall uncertainty in the measurements. Bentham spectroradiometers measure the whole UV spectrum (290 – 400 nm) with step and resolution which can be determined by the operator. The spectra from AOS and LIN (measured by Bentham spectroradiometers) used in this study have been recorded with a step of either 0.25 or 0.5 nm and a resolution of ~ 0.5 nm. The Brewer Spectrophotometer measures the total column of ozone using the differential absorption method, i.e. measuring the direct solar irradiance at four wavelengths and then comparing the intensity at wavelengths that are weakly and strongly absorbed by ozone (Kerr et al., 1985). Brewer TOC measurements are used in the present document to validate the TEMIS forecasts. The Ground-based Ultraviolet (GUV) instrument is a multichannel radiometer that measures UV radiation in five spectral bands having central wavelengths as 305, 313, 320, 340 and 380 nm. However, in addition to UV irradiances, other data that can be obtained from GUV instruments are total ozone and the cloud optical depth (Dahlback, 1996; Lakkala et al., 2018). GUV measurements are used for LAN station of Norway. At stations AKR, INN and VIE, the surface UV was measured using Solar Light (SL) 501 radiometers. It provides direct observation of UV index with a frequency of one minute. The Yankee Environmental System (YES) has been used for VAL station. The low latitude stations include AKR, ARE, ATH, ROM, THE, and VAL. AKR has minimum altitude of 23 m and VAL has maximum altitude of 705 m above sea level. The middle latitude locations are AOS, DAV, INN, BEL, LIN,

330 ~~MAN, UCC, and VIE among which the minimum altitude is 10 m in LAN and maximum altitude is in DAV at 1610 m above~~

331 ~~mean sea level. HEL, LAN, and SOD represent the high latitude zone, with HEL having an altitude of 48 m and SOD an~~

332 ~~altitude of 185 m above mean sea level (Table 2).~~

333 The low latitude stations include AKR, ARE, ATH, ROM, THE, and VAL. AKR has minimum altitude of 23 m and VAL has

334 maximum altitude of 705 m above sea level. The middle latitude locations are AOS, DAV, INN, BEL, LIN, MAN, UCC, and

335 VIE among which the minimum altitude is 10 m in LAN and maximum altitude is in DAV at 1610 m above mean sea level.

336 HEL, LAN, and SOD represent the high latitude zone, with HEL having an altitude of 48 m and SOD an altitude of 185 m

337 above mean sea level (Table 2). A summary of basic climatic information for the validation locations was obtained from the

338 Köppen climate classification (Chen and Chen, 2013) and it is summarized here. THE, AKR, ARE, ROM, ATH and VAL

339 have a Mediterranean climate comprising of mild, wet winters and dry summers. MAN experiences maritime climate (cool

340 summer and cool, but not very cold, winter). AOS, UCC, LAN, BEL, HEL, LIN and VIE experience humid continental climate

341 with warm to hot summers, cold winters and precipitation distributed throughout the year. DAV and INN experience boreal

342 climate characterised by long, usually very cold winters, and short, cool to mild summers. SOD has subarctic climate having

343 very cold winters and mild summers.

2.4 Evaluation methodology

345 The time series period covers the whole year 2017 at 15-min intervals, following the MSG available time steps. A

346 synchronization between the UVIOS simulations and the ground-based measurements was performed in order to match the

347 15-min intervals of UVIOS to the measured data. The UVIOS data availability is 93%, while for the ground stations it reaches

348 almost 79% enabling a direct UVI data comparison of 77% of the 2017 time steps. For the comparison we used the closest

349 instrument measurements to the 15-min intervals with a maximum deviation of 3 minutes in order to avoid solar elevation and

350 cloud presence mismatches. Additionally, the UVIOS comparisons included measurements up to 70 degrees SZA. The

351 rationale for this cutoff was that UVIOS retrievals at high SZA are retrieved as cloudless as COT is unavailable from MSG.

352 In addition, the comparison is also impacted by limitation of the horizon of ground-based ~~(GB)~~ sites (e.g~~.~~, Davos, Innsbruck,

353 Aosta) where the diffuse component and in some cases the direct component of solar UV irradiance are affected by obstacles

354 (mountains) on the horizon. The contribution of this mainly diffuse irradiance to the total budget is a function of solar elevation

355 and azimuth (day of the year) and also cloudiness.~~-~~ Although UVIOS simulations were corrected for changing UVI with respect

356 to altitude (see Section 3.2.3), the correction cannot be perfect for higher altitude stations. The reason is that it is not possible

357 to take into account all different factors (aerosol load and properties, atmospheric pressure, surface albedo) (e.g., Blumthaler

358 et al., 1997; Chubarova et al., 2016) which affect the change of UVI with altitude. This explains some of the deviations in the

359 results as the UVIOS retrieves UVI assuming a flat horizon. Clear sky conditions w~~h~~ere defined as the UVIOS retrieval where

360 MSG COT equals to zero. Further discussion on the uncertainties introduced by this choice is mentioned in the cloud effect

361 section.

Most of the comparisons have been performed using the absolute (mean bias or median) UVI differences (model – measurements). In addition, median values of the percentage differences (100* (model – measurements)/measurements) have been used. UVIOS estimations were also evaluated in terms of mean bias and root mean square error (MBE and RMSE, respectively), defined as follows:

$$\text{MBE} = \bar{\varepsilon} = \frac{1}{N}\sum_{i=1}^{N}\varepsilon_i \qquad (1) \qquad \text{RMSE} = \sqrt{\frac{1}{N}\sum_{i=1}^{N}\varepsilon_i^2} \qquad (2)$$

Where $\varepsilon_i = x_f - x_o$ are the residuals (UVIOS errors), calculated as the difference between the simulated values (x_f) and the ground-based values (x_o), and where N is the total number of values. MBE quantifies the overall bias and detects whether the UVIOS overestimates (MBE>0) or underestimates (MBE<0). RMSE quantifies the spread of the error distribution. Finally, the correlation coefficient (r), as well as the coefficient of determination (R^2) were used to represent the proportion of the variability between modeled and measured values.

3 Results

3.1 ~~Performance of the UVIOS technique; result overview~~Overall performance of the UVIOS system

Fig. 5 presents a scatterplot of the UVIOS simulations for all stations as compared to the ground-based measurements, which is followed by a correlation coefficient (r) of 0.944. For a more detailed view of the UVIOS performance, Fig. 6 depicts a Taylor diagram with the overall ~~UVIOS~~ model accuracy for all ground stations under all sky and clear sky conditions as a function of the correlation coefficient, normalized standard deviation and RMSE. For both, clear sky and all sky conditions, the results are similar. The absolute differences between the UVIOS and the measured UVI are within ± 0.5, and the correlation coefficients are between 0.85 and 0.99 for all stations. The RMSE is for most stations less than 0.5. ~~Under clear sky conditions, the UVIOS shows the best results with a correlation coefficient (r) close to 0.98 for THE, ROM, AKR, ARE, AOS, and VAL, while the RMSE is below 0.5 UVI for the majority of stations.~~ Under all sky conditions~~,~~ the ~~error increases with~~RMSE is higher ~~uncertainties~~relative to the RMSE for clear skies for~~at~~ MAN, DAV and SOD, which is probably ~~caused~~due to~~by~~ misclassification of cloudy pixels (see also the Appendix A section). ~~For both, clear sky and all sky conditions, the RMSE of the absolute UVI differences between the model and the measurement is close to 0 (within ± 0.5 UVI) for all stations. Most of the comparisons are provided comparing UV Index median values and not percentages. Averaging percentage~~Relative differences can be misleading as they may correspond to very small absolute differences without physical meaning, especially for low levels of the UVI~~does not provide a fair estimation of the model as such differences in most of the cases are not represented by a normal distribution and also small UVI differences (especially in high cloudiness instants and high solar angles - e.g. differences less than 1 UVI having UVI values less than 1) can differ by up to 500%~~. Thus, we ~~have~~ focused on absolute differences in order to have a more representative assessment of the actual effect (UV Index) and its results. The differences were categorized to ~~based on~~ low (less than 0.5), moderate (0.5 - 1) and high (more than 1~~2~~). ~~UVI differences~~

392 between UVIOS and the ground based measurements. However, iIn the Appendix A relative differences arewe also discussed
393 provide such differences in percent.

394 In Table 3, U1.0 and U0.5 represent the percentage of cases with absolute differences between modelled and ground based
395 UVI measurements within 1 and 0.5, respectively, for all comparisons between the 15-minute model retrievals and the
396 corresponding ground-based measurements. As shown in Table 3, for all stations and for both, clear- and all sky conditions,
397 differences were within 0.5 UVI for at least 70% of the cases. Under clear sky conditions, AOS, BEL, HEL, LAN, LIN, SOD
398 and THE had above 90% of U0.5 cases, while others have 75-90% of U0.5 cases. All stations but DAV had above 90% of
399 U1.0 cases for clear skies, while the correlation coefficients for most of the stations were above 0.9 (exceptions are ATH and
400 MAN). For all-skies differences were within 1 UVI for 90% of the cases for all stations with the correlation coefficients
401 exceeding 0.9 for most of them (exceptions are DAV, MAN and SOD). Median differences for all skies for every station were
402 well within ± 0.2 UVI, with the 25-75 percentiles being within ± 0.5 UVI and the 5-95 percentiles within ± 1 UVI.. For clear
403 skies the corresponding values are ± 0.1, ± 0.4 and ± 0.8 respectively. In the following sections we try to investigate the factors
404 that contribute to the differences between UVIOS and ground-based measurements.

405 **3.2 Factors affecting UVIOS retrievals**

406 **3.2.1 Ozone effect**

407 All the available collocated Total Ozone Column (TOC) measurements for the stations used in UVIOS evaluation have been
408 obtained from the WOUDC (https://woudc.org/) database. In this database 8 out of 17 UVIOS evaluation stations (AOS, ATH,
409 DAV, MAN, ROM, SOD, THE and UCC) were found, providing TOC ground-basedGB measurements. TOC comparison has
410 been performed by calculating daily means of ground-basedGB measurements and the TOC from TEMIS. In order to quantify
411 the effect of the uncertainty of the forecasted TOC used as input at UVIOS we have calculated the mean differences of the
412 forecasted and measured TOCs and used a radiative transfer model to investigate their effect on UVIOS retrieved UVI. Table
413 4 shows the mean differences in D.U. from TEMIS TOC (used as inputs in UVIOS) as compared to the WOUDC ground-
414 based measurements for one year of comparison data. It is seen that for the stations AOS, DAV, MAN and UCC the values of
415 the TEMIS observations are higher as compared to the ground-based measurements (by 7.6, 1.9, 5, and 2.9 DU respectively)
416 while for the other stations TEMIS observations are lower (by 0.9, 5.4, 9.9, and 2.2 DU for ATH, ROM, SOD, and THE
417 respectively). The negative bias is seen to be highest for ROM station (-9.9) and the positive bias is highest for AOS station
418 (7.6). Part of the large differences over the complex terrain sites can be explained by the difference between the actual altitude
419 of the station and the average altitude of the corresponding grid points of TEMIS. For example, for AOS the average altitude
420 of the pixel is 2000 m while the real altitude of the station is 570 m, resulting in an underestimation of the tropospheric column
421 of ozone by TEMIS. In general, differences can be explained by the combined effects of uncertainties in TOC retrieval from
422 satellite and ground-basedGB platforms (Rimmer et al., 2018; Boynard et al., 2018; Garane et al., 2018). Figure 76 shows the
423 effect of this TOC bias on the calculated UVIOS. As seen in Table 4, there is a mix of small underestimation and overestimation

cases in the TOCs used within UVIOS, with average absolute differences of 4-5 DU. Worst TOC UVIOS inputs were found in AOS and ROM (7.6 and -9.9 DU) leading to maximum (at 30 degrees SZA) differences in UVI of -0.22 and 0.3 for AOS and ROM, respectively. In general, in most of the cases UVI mean differences are less than 0.1. It has to be noted that the TOC differences have a larger impact when expressed in percent at higher SZAs, while in Figure 76 higher absolute differences for low SZA's are associated with higher UVIs at these SZAs. Detailed comparisons for each station are shown in the Appendix A figures.

3.2.2 Aerosol effect

Aerosol optical depth measurements used for the UVIOS aerosol input evaluation have been collected from the AERONET-NASA web site (Giles et al., 2019) for 12 out of our total 17 stations (AKR, ARE, ATH, DAV, HEL, LIN, ROM, SOD, THE, UCC, VAL and VIE. AERONET (level 2, version 3) values of AOD at 500 nm were interpolated at 550nm using the AERONET derived 440-870nm Angstrom exponent for each individual measurement. In order to compare those measurements with CAMS forecasted AOD used for the UVIOS their daily means were derived. The comparison of forecasted and measured daily means was based on all available data due to gaps in the AERONET time series. The AOD MBE and RMSE statistical scores are shown in Table 5 in absolute units and correlation coefficient as well. All the stations have a mean positive bias up to 0.071 except UCC which is showing a mean negative bias of 0.007. The comparison of all individual stations with CAMS data used as inputs on UVIOS showed that under all cases CAMS AOD is higher than that from AERONET with a mean difference of 0.07 at 550nm. The correlation between the modeled and the measured values varies from 0.10 for VIE to 0.91 for ARE with most of the stations showing the correlation coefficient above 0.7. As in the case of the TOC, AOD CAMS data are forecasts from the previous day and real time WOUDC or AERONET level 2.0 data do not exist. Although real time TOC (and in due course AOD in the UV) is available from Eubrewnet (López-Solano et al., 2018; Rimmer et al., 2018), it is only for particular locations and not for the whole European domain. Thus, the only choice in providing for a real time UV Index for Europe is using the CAMS (for AOD) and the TEMIS (for TOC) data.

In order to evaluate the effect of AOD on UVI, UVI differences between the UVIOS using both AOD datasets (CAMS and AERONET) as UVIOS inputs were analyzed. Figure 87 shows the mean bias error of the CAMS – AERONET AOD impact on UVI for all stations with available ground based AOD data as a function of SZA together with the uncertainty range (± 1 σ). It can be seen that UVIOS with CAMS AOD input underestimates UVI compared to the UVIOS with AERONET data, except for the UCC station. This is consistent with CAMS overestimations of AOD compared to the AERONET measurements, except for the station UCC as shown in Table 5. Higher aerosol levels in the atmosphere tend to lower the UVI. Highest difference in UVI is observed for the stations HEL, SOD, VIE. Since, the aerosol level at the stations HEL and SOD is very low, the percent difference between the AOD from CAMS and AERONET is larger for these stations (although the absolute difference is similar) relative to stations with higher AOD, leading to higher differences in the UVI. Aerosol content for VIE is higher than HEL and SOD but still within 0.2 which might be the reason for the higher UVI difference. In terms of SZA, it

is observed that the mean bias decreases with an increase in the SZA as the values of UVI also decrease with SZA and the most deviation is for station VIE which is consistent with the poor correlation between the CAMS forecasted input and the measurements for this station as seen from Table 5.

The use of single scattering albedo in the UV region is a difficult task and many studies have shown that such measurements need extra effort and it is not possible to perform them worldwide (Arola et al., 2009; Kazadzis et al., 2016; Raptis et al., 2018). The monthly values of the single scattering albedo used in UVIOS for the UV region were derived from the MACv2 database at the 310 nm wavelength (Kinne, 2019). Fig 98 shows the intra annual variability of SSA for the 17 stations. For all stations, SSA values range from 0.76 to 0.93, with most of them having SSA values between 0.83 to 0.93, and relatively small variability. In contrast, there are stations like ARE, BEL, INN, LIN, VIE and THE which have relatively smaller SSA values (0.76-0.9) and greater variability than the other stations.

3.2.3 Albedo effect & surface elevation correction

Surface albedo at UV wavelengths is small (2 – 5%) for most types of surfaces (Feister and Grewe, 1995; Madronich, 1993) except for features like sand (with a typical albedo of ~0.3) and snow (up to 1 for fresh snow) (Meinander et al., 2013; Myhre and Myhre, 2003; Vanicek et al., 2000; Henderson-Sellers and Wilson, 1983). Renaud et al. (2000), found an enhancement of about 15 to 25% in UVI for clear-skies and snow conditions due to the multiple ground-atmosphere reflections and this relative increment was about 80% larger for overcast conditions. The combined effect of aerosols and snow lead to an enhancement of about 50% in UVI in cloud-free condition for moderately polluted atmospheres (Badosa and Van Weele, 2002). Fig. 10 (a)9 presents the effect of surface albedo on the UVI percentage difference (i.e. for various albedo values under clear sky conditions) as a function of SZA, while Fig. 10 (b) shows the effect of surface elevation on UVI as a function of the percentage difference for various total ozone columns. It is observed that the UVI percentage difference increases almost linearly with albedo for a particular SZA and the variation is found to be almost identical for all SZA. This indicates that the UVI percentage difference is independent of the SZA and increases with surface albedo. The UVI percentage difference is found also to increase almost linearly with the increase in elevation for a particular total ozone column. The percentage difference is similar for all ozone columns up to 1km, after which the differences with ozone column become more apparent. That is, at a particular elevation, the percentage difference is higher for less total ozone column. A 1% fluctuation (decline or increase) in column ozone can lead to about a 1.2% fluctuation (increase or decline) in the UV Index (Fioletov et al., 2003; Probst et al., 2012). Indicatively, the average maximum surface elevation correction in terms of UVI for the DAV station (due to UVIOS input deviation from to actual elevation) was of the order of 1.6 (15%), while for INN and AOS it was 0.5 and 0.6 respectively (6%) and for the VAL station close to 0.8 (8%).

Uncertainties introduced in UVIOS from the use of a constant surface albedo value of 0.05 for non-snow conditions are quite low. For the case of albedo values used for snow conditions based on the CGLS monthly mean product uncertainties can be related to: the small difference of UV and visible albedo values; the fact that the CGLS provides an albedo of a certain area

around the station that does not necessarily coincide with the "effective" albedo area affecting UV measurements; and finally that the monthly albedo product represents a monthly average while a real time CGLS product represents the last 12 days (dynamically changing albedo). In order to investigate this last point, we have compared the UV effects from the use of the two albedo datasets for DAV station, where the average difference between an example ground-based dataset and UVIOS was found to be 0.14 UVI (Gröbner, 2021). In Fig. 11̶0̶, the effect of surface albedo correction is shown for the Davos station, for a period with snow cover and low percentage cloudiness. The climatological and the dynamically changing albedo are presented in terms of percentage differences between modelled and ground measurements as a function of SZA. In the case of climatological albedo, most of the percentage difference between forecasted and the measured UVI value is found to vary from -30% to 10% for SZA between 20° to 70°, showing more underestimation than overestimation from the UVIOS simulations. Similarly, in the case of dynamically changing albedo, most of the percentage difference between forecasted and the measured UVI value is found to vary from -20% to 10% for SZA between 20° to 70°. The mean percentage difference between the results using the two different albedo inputs is -2.76% in terms of accuracy improvement. However, beyond 70 degree SZA, there is a huge variation in the percentage difference with mostly underestimations from the UVIOS simulations (not shown in Fig. 11̶0̶).

3.2.4 Cloud effect

For the evaluation we used measurements at SZA lower than 70 degrees, based on the lack of cloud input from MSG for higher SZAs. The lack of MSG data results in an overestimation of UVIOS in high SZAs and the UVI is systematically overestimated for long periods during winter at high latitude regions when SZA does not get below 70 degrees during the day. However, based on the simulations performed by UVIOS, this overestimation is low in terms of absolute UVI and does not usually exceed 0.2 UVI because maximum UVIs at such SZAs rarely exceed UVI=1.

COT retrieved from the MSG satellite has been used as input for the UVIOS together with typical optical properties of the clouds as discussed in Sect. 2.1. The evaluation of all stations for cloudless and cloudy conditions can be seen in Figure 12̶1̶ that shows the relative frequency distribution of all stations (colours) and the mean (black line) for cloudless (upper plot) and cloudy conditions (lower plot). Mean bias error of the modeled by UVIOS and measured UVI for all- and clear sky conditions and the percentage of clear sky time steps data is presented in Figure 13̶2̶. The mean bias for clear sky conditions is found to be less than that for the all sky conditions for the stations AKR, ATH and THE (having most days of the year being cloudless as the clear sky percentage is above 70%). The MBE for DAV, LIN and MAN is less for clear sky relative to all sky conditions even though most days of the year are cloudy (clear sky annual percentage less than 45%) at the particular stations. While, stations BEL, HEL, INN, LAN, SOD, UCC and VIE, that have mostly cloudy skies throughout the year (clear sky annual percentage less than 50%), are having more MBE for clear sky conditions than the all sky condition. This can be due to the erroneous classification of a cloudy sky as clear sky, which is also discussed in the following section. MBE is also larger for

519   AOS and ARE which have mostly clear skies throughout the year. Stations ROM and VAL have comparatively much smaller

520   MBE for clear sky conditions.

521   As shown in Table 6 there are 45.4% of cases with underestimations and 54.6% cases with overestimations for cloudless

522   conditions (COT=0). For all the other cases, overestimations (62.5%) are more predominant than underestimations (37.5%).

523   The difference in the modelled and the measured values goes beyond ± 1 UVI for only 5.1% cases for cloudless conditions

524   and 14.7% for all other cases. In general, under cloudy conditions, UVIOS shows an overestimation for UVI in contrast to the

525   ground measurements. One explanation for the overestimations could be the erroneous determination of COT from MSG above

526   the ground-based stations, giving cloud input that can be overestimated or underestimated. The results show that there is a

527   general tendency for a small underestimation of MSG COT that leads to a systematic but small UVIOS UVI overestimation

528   under cloudy conditions. Another possible explanation is the spatial representativeness of MSG COT. The MSG COT

529   determination is available at 5 by 5 km pixels that may differ from the actual situation of the cloud prevailing above the station,

530   especially in broken cloud conditions and ~~in~~a case when it blocks the direct radiation from the sun. Moreover, for lower solar

531   elevations, the direct sun irradiance can be blocked by cloud in neighbouring pixels. The first effect has been explored in the

532   relative frequency distribution of Figure 12~~1~~ that shows a higher number (~ 63%) of data on the right of the zero UVI difference

533   vertical line for cloudy skies. When comparing data outside the 0.5 and 1 difference limits we also see that $1 - 4$ times more

534   data show a UVIOS overestimation as compared to the clear sky case. This shows that in general there is a small (in UVI

535   terms) but significant UVIOS overestimation for non-zero COT conditions. Moreover, for clear skies, as determined from the

536   MSG, we observe a less pronounced UVIOS overestimation that corresponds to the fact that even if MSG defines the situation

537   as completely cloudless, in reality there may be some cases where clouds near the ground-based~~GB~~ station affect the measured

538   UVI. This effect is easier to understand when showing these differences as a function of solar zenith angle which is explored

539   through Figure 14~~3~~. It is observed that the absolute difference between the modelled and the measured values decreases with

540   increasing solar zenith angle and most of the difference lies within ± 4 UVI. The seasonal variation of the percentage UVI

541   difference as a function of SZA shows that while absolute UVI is small in winter the percentage difference is higher compared

542   to other seasons.

543   Figure 15~~4~~ (a) shows the shadow volume at the surface level of a cloud, relative to the SEVIRI angle view, as a function of

544   cloud height and SZA, highlighting the ray tracing in the presence of clouds and the accompanied angular dependence due to

545   the 3D geometry.~~surface horizontal distance as a function of the cloud height and the SZA required for the cloud to block the~~

546   ~~sun.~~ 15~~4~~ (b) shows the scatter of the UVI difference under clear sky conditions for all stations as a function of SZA. It is

547   observed that there is an obvious pattern of scattered data for UVI differences higher than 1.5 compared with the ones for

548   differences less than -1.5. These data represent UVIOS overestimation for UVI retrievals due to the underestimation of the

549   cloudiness just above the stations. These data illustrate the well-known spatial representativeness issues whereby a COT value

550   for a satellite grid is not fully representative of a point measurement station. In addition, absolute and percentage relative

551   differences are shown in Fig. 15~~4~~ (c) and (d) respectively for SZA up to 65 degrees. The differences between the UVIOS and

552   the ground-based~~GB~~ UVI decreases in absolute level but increases in percent with an increase in SZA. This is due to the

553 decrease of UVI with increasing SZA. Modelled and the measured UVI difference is close to zero both for mean and median

554 values. For SZA below 30 degrees, differences are 0 to -0.2, while 20 to 80 percentiles range from -0.6 to -0.2. Percentage

555 difference increases with SZA as absolute UVI decreases with the 20 to 80 percentiles showing differences between -10%

556 and 10%

557 ~~3.2.5 Surface elevation correction~~

558 ~~Fig. 15 presents the effect of surface elevation on UVI as a function of the percentage difference for various total ozone~~

559 ~~columns. The UVI percentage difference is found to increase almost linearly with the increase in elevation for a particular total~~

560 ~~ozone column. The percentage difference is similar for all ozone columns up to 1km, after which the differences with ozone~~

561 ~~column become more apparent. That is, at a particular elevation, the percentage difference is higher for less total ozone column.~~

562 ~~A 1% fluctuation (decline or increase) in column ozone can lead to about a 1.2% fluctuation (increase or decline) in the UV~~

563 ~~Index (Fioletov et al., 2003; Probst et al., 2012). Indicatively, the surface elevation correction in UVI for the DAV station (due~~

564 ~~to UVIOS input deviation from to actual elevation) was of the order of 15%, while for INN and AOS it was 6% and for the~~

565 ~~VAL station close to 8%.~~

566 **4. Summary and conclusions**

567 In this study, a fast RTM model of UVI, the so-called UVIOS, using inputs of the SZA, aerosol optical depth, total ozone

568 column, cloud optical depth, elevation and surface albedo that implicitly includes temporal effects and the effect of cloud and

569 aerosol physics, allows for the generation of high-resolution maps of UVI. Ground based measurements of UV are the most

570 accurate way to determine this important health related parameter. However, such stations are sparse and hence, satellite

571 observations can be used in order to have a nowcasted UV service. To date polar orbiting satellites like TOMS, OMI and

572 recently TROPOMI provided a global UV dataset with a major disadvantage being the temporal resolution (one measurement

573 per day). This, combined with the large temporal variability of clouds can lead to huge deviations from reality when a single

574 daily measurement is included. Geostationary satellite, MSG, have been used in order to try to improve on such limitations

575 using cloud information every 15 minutes.

576 Comparison of the forecasted and the ground-based measurements indicated that at least 70% and 80% of comparisons were

577 within 0.5 UVI difference for all sky condition and clear sky, respectively. The mean differences TEMIS TOC and the ground

578 measured TOC from the WOUDC for one year of comparison data showed that TEMIS tends to slightly overestimate the TOC

579 for some stations along with underestimating it for other stations. While, in general, in most of the cases UVI mean differences

580 are less than 0.1, the TOC differences have a larger impact in percent UVI differences at higher SZAs. Such small differences

581 can also be the result of daily TOC variation not captured in TEMIS.

CAMS AOD seems to be slightly overestimated as compared with AERONET data that leads to a UVIOS underestimation. CAMS data are found to overestimate the AOD from AERONET measurements with a mean difference of 0.07 at 500 nm. All the stations have a mean positive bias up to 0.071 except one station that had a mean negative bias of 0.007. The analysis of the impact of the mean bias error of the CAMS – AERONET AOD impact on UVI for all stations showed that the mean bias decreases with an increase in the SZA as the values of UVI also decreases with SZA. The greatest deviation is for station VIE which is consistent with the poor correlation between the CAMS forecasted input and the measurements for this station. The real time data provision approach of UVIOS requires using a maximum of one-day ozone and aerosol forecast using the TEMIS and CAMS service respectively. Uncertainties in the used SSA increase the overall uncertainty of the simulated UVI, especially for high levels of atmospheric aerosols. However, as systematic SSA measurements in the UV region are not available, quantification of these uncertainties were not possible.

Cloudy conditions show high percentage differences but low UVI differences, and have a general tendency to lead to a UVIOS overestimation. It was found that 45.4% of cases have underestimations while 54.6% cases have overestimations for the cloudless conditions, while overestimations (62.5%) were more predominant than underestimations (37.5%) for all the other cases. In general, UVIOS showed an overestimation for UVI in contrast to the ground measurements under cloudy conditions with the difference in the modeled and the measured values going beyond ±1 for 5.1% cases for cloudless conditions and 14.7% for all other cases. At individual stations the results for cloudless sky conditions, which are the most important for health related issues, showed good agreement. In general, ~85% of all and 95% of cloudless cases are within 1 UVI difference. The relative percentage biases can be large for low UVI cases due to clouds or at high SZAs, above 75°, due to the absence of accurate information for clouds. The results show that there is a general tendency of small underestimation of MSG COT that leads to a systematic but small UVIOS overestimation under cloudy conditions. Another possible explanation is the spatial representativeness issues between a satellite and a single point on the ground.

SSA validation is difficult to perform as there are no systematic SSA measurements in the UV region. Using climatological surface albedo has little impact at low albedo sites but mainly leads to underestimations in UVIOS simulations for high albedo situations (snow cover). Most of the percentage difference between forecasted and the measured UVI values varied from -30% to 10% for SZA between 20° to 70° (climate albedo), while it was found to vary from -20% to 10% for dynamically changing albedo. Since high surface albedo conditions correspond to winter months (i.e. high SZAs and relatively low UVI) for the stations used in the study, the corresponding absolute differences in the UVI are generally smaller than 2 UVI. However, there was a huge variation in the percentage difference beyond 70 degree SZA with mostly underestimations from the UVIOS simulations. Finally, for uncertainties in elevation inputs, the UVI percentage difference is found to increase almost linearly with the increase in elevation for a particular total ozone column and beyond that, it is seen that the rate of increase in the percentage difference decreases with increase in the total ozone column.

UVIOS system forms a novel tool for widespread estimations of UVI using real-time and forecasted EO inputs. UVIOS utilizes the MSG domain with high spatiotemporal resolution, producing outputs within acceptable limits of accuracy for UV health related applications. It captures basic cloud features and all major atmospheric and geospatial parameters that affect UVI.

616 Under cloudless conditions it performs to within the uncertainty of the ground based measurements to which it has been
617 compared. Further development and improvement of the model can be achieved in the future. Meteosat Third Generation
618 (MTG) satellites are expected to be launched in the following years and give aerosol and cloud products which would improve
619 the performance of nowcast and forecast UV models when used as inputs. A future goal is to compare the UVIOS accuracy
620 under cloudy conditions by using, (i) the current MSG cloud information (5 km, 15 min), (ii) the ECMWF forecast cloud
621 information (4 km, 1 hour) and (iii) the forthcoming MTG cloud information (500m, 5 min), in order to quantify the
622 uncertainties of the forecasted cloud data as compared to the satellite observations, as well as the overall improvement of the
623 MTG data compared to the MSG due to the MTG's higher resolution.
624

Author contribution

626 PGK was responsible for the design of the study and the whole analysis, with support from SK, AWS, PIR, KP, IF, AM and
627 J.G. PGK and SK are the developers of UVIOS. All authors contributed to editing the paper.

Code/Data availability

629 All data used as inputs to the UVIOS system are open access, while all data sets produced by the UVIOS for the purposes of
630 this paper can be requested from the corresponding author. The ground-based measurements can be requested from the PIs of
631 the stations. The UVIOS suite of algorithms and LUTs can be used for various applications after consultation with the
632 corresponding author.

Competing interests

634 The authors declare that they have no conflict of interest.

Acknowledgements

We acknowledge the Eumetsat SAFNWC, the Copernicus and TEMIS services as well as the Aerocom and GOME teams for providing all the necessary data used in this study. We would like to thank the 17 site instrument operators and technical staff that made the ground based measurements feasible.

Financial support

The UVIOS development received no specific grant from any funding agency in the public, commercial, or not-for-profit sectors. The evaluation part of this study has been partly funded by the European Commission project EuroGEO e-shape (grant agreement No 820852).

References

Andrady, A.L., Aucamp, P.J., Austin, A.T., Bais, A.F., Ballare, C.L., Barnes, P.W., Bernhard, G.H., Bornman, J.F., Caldwell, M.M., de Gruijl, F.R., and Erickson, D.J.: Environmental effects of ozone depletion and its interactions with climate change: 2014 assessment executive summary. Photochemical and Photobiological Sciences 14(1), 14-18, 10.1039/c4pp90042a, 2015.

Arola, A., Kazadzis, S., Lindfors, A., Krotkov, N., Kujanpää, J., Tamminen, J., Bais, A., di Sarra, A., Villaplana, J. M., Brogniez, C., Siani, A. M., Janouch, M., Weihs, P., Webb, A., Koskela, T., Kouremeti, N., Meloni, D., Buchard, V., Auriol, F., Ialongo, I., Staneck, M., Simic, S., Smedley, A., and Kinne, S.: A new approach to correct for absorbing aerosols in OMI UV, Geophysical Research Letters, 36, 10.1029/2009gl041137, 2009.

Badosa, J., and Van Weele, M.: Effects of aerosols on UV-index, KNMI Scientific Report WR-2002-07, 2002.

Badosa, J., Calbó, J., McKenzie, R., Liley, B., González, J.-A., Forgan, B., and Long, C. N.: Two Methods for Retrieving UV Index for All Cloud Conditions from Sky Imager Products or Total SW Radiation Measurements, Photochemistry and Photobiology, 90, 941-951, https://doi.org/10.1111/php.12272, 2014.

Bais, A. F., Zerefos, C. S., Meleti, C., Ziomas, I. C., and Tourpali, K.: Spectral measurements of solar UVB radiation and its relations to total ozone, SO2, and clouds, Journal of Geophysical Research: Atmospheres, 98, 5199-5204, 10.1029/92jd02904, 1993.

Bais, A. F., Lucas, R. M., Bornman, J. F., Williamson, C. E., Sulzberger, B., Austin, A. T., Wilson, S. R., Andrady, A. L., Bernhard, G., McKenzie, R. L., Aucamp, P. J., Madronich, S., Neale, R. E., Yazar, S., Young, A. R., de Gruijl, F. R., Norval, M., Takizawa, Y., Barnes, P. W., Robson, T. M., Robinson, S. A., Ballaré, C. L., Flint, S. D., Neale, P. J., Hylander, S., Rose, K. C., Wängberg, S. Å., Häder, D. P., Worrest, R. C., Zepp, R. G., Paul, N. D., Cory, R. M., Solomon, K. R., Longstreth, J., Pandey, K. K., Redhwi, H. H., Torikai, A., and Heikkilä, A. M.: Environmental effects of ozone depletion, UV radiation and interactions with climate change: UNEP Environmental Effects Assessment Panel, update 2017, Photochemical & Photobiological Sciences, 17, 127-179, 10.1039/c7pp90043k, 2018.

Bais, A. F., Bernhard, G., McKenzie, R. L., Aucamp, P. J., Young, P. J., Ilyas, M., Jöckel, P., and Deushi, M.: Ozone–climate interactions and effects on solar ultraviolet radiation, Photochemical & Photobiological Sciences, 18, 602-640, 10.1039/c8pp90059k, 2019.

Bernhard, G.: Trends of solar ultraviolet irradiance at Barrow, Alaska, and the effect of measurement uncertainties on trend detection, Atmos. Chem. Phys., 11, 13029-13045, 10.5194/acp-11-13029-2011, 2011.

Bernhard, G., and Stierle, S.: Trends of UV Radiation in Antarctica, Atmosphere, 11, 10.3390/atmos11080795, 2020.

Bieliński, T.: A Parallax Shift Effect Correction Based on Cloud Height for Geostationary Satellites and Radar Observations, Remote Sensing, 12, 10.3390/rs12030365, 2020.

Blumthaler, M., and Ambach, W.: SOLAR UVB-ALBEDO OF VARIOUS SURFACES, Photochemistry and Photobiology, 48, 85-88, https://doi.org/10.1111/j.1751-1097.1988.tb02790.x, 1988.

Blumthaler, M., Ambach, W., and Ellinger, R.: Increase in solar UV radiation with altitude, Journal of Photochemistry and Photobiology B: Biology, 39, 130-134, https://doi.org/10.1016/S1011-1344(96)00018-8, 1997.

Boynard, A., Hurtmans, D., Garane, K., Goutail, F., Hadji-Lazaro, J., Koukouli, M. E., Wespes, C., Vigouroux, C., Keppens, A., Pommereau, J. P., Pazmino, A., Balis, D., Loyola, D., Valks, P., Sussmann, R., Smale, D., Coheur, P. F., and Clerbaux, C.: Validation of the IASI FORLI/EUMETSAT ozone products using satellite (GOME-2), ground-based (Brewer–Dobson, SAOZ, FTIR) and ozonesonde measurements, Atmos. Meas. Tech., 11, 5125-5152, 10.5194/amt-11-5125-2018, 2018.

~~Calbó, J., Pagès, D., and González, J. A.: Empirical studies of cloud effects on UV radiation: A review, Reviews of Geophysics, 43, 10.1029/2004rg000155, 2005.~~

Carrer, D., Roujean, J.-L., and Meurey, C.: Comparing Operational MSG/SEVIRI Land Surface Albedo Products From Land SAF With Ground Measurements and MODIS, IEEE Transactions on Geoscience and Remote Sensing, 48, 1714-1728, 10.1109/TGRS.2009.2034530, 2010.

Cede, A., Herman, J., Richter, A., Krotkov, N., and Burrows, J.: Measurements of nitrogen dioxide total column amounts using a Brewer double spectrophotometer in direct Sun mode, Journal of Geophysical Research: Atmospheres, 111, https://doi.org/10.1029/2005JD006585, 2006.

Chubarova, N., Zhdanova, Y., and Nezval, Y.: A new parameterization of the UV irradiance altitude dependence for clear-sky conditions and its application in the on-line UV tool over Northern Eurasia. Atmos. Chem. Phys., 16, 11867-11881, 10.5194/acp-16-11867-2016, 2016.

Chubarova, N.E., Pastukhova, A.S., Zhdanova, E.Y., Volpert, E.V., Smyshlyaev, S.P., and Galin, V.Y.: Effects of ozone and clouds on temporal variability of surface UV radiation and UV resources over Northern Eurasia derived from measurements and modeling. Atmosphere, 11(1), 59, 10.3390/atmos11010059, 2020.

Corr, C. A., Krotkov, N., Madronich, S., Slusser, J. R., Holben, B., Gao, W., Flynn, J., Lefer, B., and Kreidenweis, S. M.: Retrieval of aerosol single scattering albedo at ultraviolet wavelengths at the T1 site during MILAGRO, Atmos. Chem. Phys., 9, 5813-5827, 10.5194/acp-9-5813-2009, 2009.

Czerwińska, A. E., Krzyścin, J. W., Jarosławski, J., and Posyniak, M.: Effects of urban agglomeration on surface-UV doses: a comparison of Brewer measurements in Warsaw and Belsk, Poland, for the period 2013–2015, Atmos. Chem. Phys., 16, 13641-13651, 10.5194/acp-16-13641-2016, 2016.

Dahlback, A.: Dahlback, Measurements of biologically effective UV doses, total ozone abundances, and cloud effects with multichannel, moderate bandwidth filter instruments, Appl. Opt. Vol. 35, No. 33, 1996. Further references, see. Eg. Bernhard et al, Johnsen et al. JGR, 2008, Applied Optics, 35, 6514 - 6521, 10.1364/AO.35.006514, 1996.

De Bock, V., De Backer, H., Van Malderen, R., Mangold, A., and Delcloo, A.: Relations between erythemal UV dose, global solar radiation, total ozone column and aerosol optical depth at Uccle, Belgium, Atmos. Chem. Phys., 14, 12251-12270, 10.5194/acp-14-12251-2014, 2014.

Derrien, M., and Le Gléau, H.: MSG/SEVIRI cloud mask and type from SAFNWC, International Journal of Remote Sensing, 26, 4707-4732, 10.1080/01431160500166128, 2005.

Eleftheratos, K., Kazadzis, S., Zerefos, C. S., Tourpali, K., Meleti, C., Balis, D., Zyrichidou, I., Lakkala, K., Feister, U., Koskela, T., Heikkilä, A., and Karhu, J. M.: Ozone and Spectroradiometric UV Changes in the Past 20 Years over High Latitudes, Atmosphere-Ocean, 53, 117-125, 10.1080/07055900.2014.919897, 2015.

Eskes, H., Huijnen, V., Arola, A., Benedictow, A., Blechschmidt, A. M., Botek, E., Boucher, O., Bouarar, I., Chabrillat, S., Cuevas, E., Engelen, R., Flentje, H., Gaudel, A., Griesfeller, J., Jones, L., Kapsomenakis, J., Katragkou, E., Kinne, S., Langerock, B., Razinger, M., Richter, A., Schultz, M., Schulz, M., Sudarchikova, N., Thouret, V., Vrekoussis, M., Wagner, A., and Zerefos, C.: Validation of reactive gases and aerosols in the MACC global analysis and forecast system, Geosci. Model Dev., 8, 3523-3543, 10.5194/gmd-8-3523-2015, 2015.

Eskes, H. J., Velthoven, P. F. J. V., Valks, P. J. M., and Kelder, H. M.: Assimilation of GOME total-ozone satellite observations in a three-dimensional tracer-transport model, Quarterly Journal of the Royal Meteorological Society, 129, 1663-1681, https://doi.org/10.1256/qj.02.14, 2003.

Eskes, H. J., Wagner, A., Schulz, M., Christophe, Y., Ramonet, M., Basart, S., Benedictow, A., Bennouna, Y., Blechschmidt, A.-M., Chabrillat, S., Clark, H., Cuevas, E., Flentje, H., Hansen, K. M., IM, U., Kapsomenakis, J., Langerock, B., Petersen, K., Richter, A., Sudarchikova, N., Thouret, V., Warneke, T., and Zerefos, C.: Validation report of the cams near-real-time global atmospheric composition service: period September-November 2017., Copernicus Atmosphere Monitoring Service (CAMS) Report, CAMS84_2015SC3_D84.1.1.10_2017SON_V1.pdf, February 2018., 2018.

Feister, U., and Grewe, R.: SPECTRAL ALBEDO MEASUREMENTS IN THE UV and VISIBLE REGION OVER DIFFERENT TYPES OF SURFACES, Photochemistry and Photobiology, 62, 736-744, https://doi.org/10.1111/j.1751-1097.1995.tb08723.x, 1995.

Fioletov, V., Kerr, J. B., and Fergusson, A.: The UV Index: Definition, Distribution and Factors Affecting It, Canadian Journal of Public Health, 101, I5-I9, 10.1007/bf03405303, 2010.

Fioletov, V. E., Kerr, J. B., McArthur, L. J. B., Wardle, D. I., and Mathews, T. W.: Estimating UV Index Climatology over Canada, Journal of Applied Meteorology and Climatology, 42, 417-433, 10.1175/1520-0450(2003)042<0417:EUICOC>2.0.CO;2, 2003.

Fioletov, V. E., McArthur, L. J. B., Mathews, T. W., and Marrett, L.: On the relationship between erythemal and vitamin D action spectrum weighted ultraviolet radiation, Journal of Photochemistry and Photobiology B: Biology, 95, 9-16, https://doi.org/10.1016/j.jphotobiol.2008.11.014, 2009.

Fioletov, V.E., Griffioen, E., Kerr, J.B., Wardle, D.I., and Uchino, O.: Influence of volcanic sulfur dioxide on spectral UV irradiance as measured by Brewer spectrophotometers. Geophysical Research Letters, 25(10), 1665-1668, 1998.

738 Fountoulakis, I., Bais, A. F., Fragkos, K., Meleti, C., Tourpali, K., and Zempila, M. M.: Short- and long-term variability of
739 spectral solar UV irradiance at Thessaloniki, Greece: effects of changes in aerosols, total ozone and clouds, Atmos. Chem.
740 Phys., 16, 2493-2505, 10.5194/acp-16-2493-2016, 2016.

741 Fountoulakis, I., Zerefos, C. S., Bais, A. F., Kapsomenakis, J., Koukouli, M.-E., Ohkawara, N., Fioletov, V., De Backer, H.,
742 Lakkala, K., Karppinen, T., and Webb, A. R.: Twenty-five years of spectral UV-B measurements over Canada, Europe and
743 Japan: Trends and effects from changes in ozone, aerosols, clouds, and surface reflectivity, Comptes Rendus Geoscience, 350,
744 393-402, https://doi.org/10.1016/j.crte.2018.07.011, 2018.

745 Fountoulakis, I., Natsis, A., Siomos, N., Drosoglou, T., and Bais, F. A.: Deriving Aerosol Absorption Properties from Solar
746 Ultraviolet Radiation Spectral Measurements at Thessaloniki, Greece, Remote Sensing, 11, 10.3390/rs11182179, 2019.

747 Fountoulakis, I., Diémoz, H., Siani, A.-M., Laschewski, G., Filippa, G., Arola, A., Bais, A. F., De Backer, H., Lakkala, K.,
748 Webb, A. R., De Bock, V., Karppinen, T., Garane, K., Kapsomenakis, J., Koukouli, M.-E., and Zerefos, C. S.: Solar UV
749 Irradiance in a Changing Climate: Trends in Europe and the Significance of Spectral Monitoring in Italy, Environments, 7,
750 10.3390/environments7010001, 2020a.

751 Fountoulakis, I., Diémoz, H., Siani, A. M., Hülsen, G., and Gröbner, J.: Monitoring of solar spectral ultraviolet irradiance in
752 Aosta, Italy, Earth Syst. Sci. Data, 12, 2787-2810, 10.5194/essd-12-2787-2020, 2020b.

753 Gal, S.: Computing elementary functions: A new approach for achieving high accuracy and good performance, Accurate
754 Scientific Computations, Berlin, Heidelberg, 1986, 1-16,

755 Garane, K., Bais, A. F., Kazadzis, S., Kazantzidis, A., and Meleti, C.: Monitoring of UV spectral irradiance at Thessaloniki
756 (1990–2005): data re-evaluation and quality control, Ann. Geophys., 24, 3215-3228, 10.5194/angeo-24-3215-2006,
757 2006.

758 Garane, K., Lerot, C., Coldewey-Egbers, M., Verhoelst, T., Koukouli, M. E., Zyrichidou, I., Balis, D. S., Danckaert, T.,
759 Goutail, F., Granville, J., Hubert, D., Keppens, A., Lambert, J. C., Loyola, D., Pommereau, J. P., Van Roozendael, M., and
760 Zehner, C.: Quality assessment of the Ozone_cci Climate Research Data Package (release 2017) – Part 1: Ground-based
761 validation of total ozone column data products, Atmos. Meas. Tech., 11, 1385-1402, 10.5194/amt-11-1385-2018, 2018.

762 Garane, K., Koukouli, M. E., Verhoelst, T., Lerot, C., Heue, K. P., Fioletov, V., Balis, D., Bais, A., Bazureau, A., Dehn, A.,
763 Goutail, F., Granville, J., Griffin, D., Hubert, D., Keppens, A., Lambert, J. C., Loyola, D., McLinden, C., Pazmino, A.,
764 Pommereau, J. P., Redondas, A., Romahn, F., Valks, P., Van Roozendael, M., Xu, J., Zehner, C., Zerefos, C., and Zimmer,
765 W.: TROPOMI/S5P total ozone column data: global ground-based validation and consistency with other satellite missions,
766 Atmos. Meas. Tech., 12, 5263-5287, 10.5194/amt-12-5263-2019, 2019.

767 Giles, D. M., Sinyuk, A., Sorokin, M. G., Schafer, J. S., Smirnov, A., Slutsker, I., Eck, T. F., Holben, B. N., Lewis, J. R.,
768 Campbell, J. R., Welton, E. J., Korkin, S. V., and Lyapustin, A. I.: Advancements in the Aerosol Robotic
769 Network (AERONET) Version 3 database – automated near-real-time quality control algorithm with improved cloud
770 screening for Sun photometer aerosol optical depth (AOD) measurements, Atmos. Meas. Tech., 12, 169-209, 10.5194/amt-12-
771 169-2019, 2019.

772 Gratien, A., Nilsson, E., Doussin, J.F., Johnson, M.S., Nielsen, C.J., Stenstrøm, Y., and Picquet-Varrault, B.: UV and IR
773 absorption cross-sections of HCHO, HCDO, and DCDO. The journal of Physical Chemistry, A, 111(45), 11506-11513, 2007.

774 Gröbner, J., Schreder, J., Kazadzis, S., Bais, A. F., Blumthaler, M., Görts, P., Tax, R., Koskela, T., Seckmeyer, G., Webb, A.
775 R., and Rembges, D.: Traveling reference spectroradiometer for routine quality assurance of spectral solar ultraviolet irradiance
776 measurements, Applied Optics, 44, 5321-5331, 10.1364/ao.44.005321, 2005.

Gröbner, J., and Sperfeld, P.: Direct traceability of the portable QASUME irradiance scale to the primary irradiance standard of the PTB, Metrologia, 42, 134-139, 10.1088/0026-1394/42/2/008, 2005.

Gröbner, J., Kröger, I., Egli, L., Hülsen, G., Riechelmann, S., and Sperfeld, P.: The high-resolution extraterrestrial solar spectrum (QASUMEFTS) determined from ground-based solar irradiance measurements, Atmos. Meas. Tech., 10, 3375-3383, 10.5194/amt-10-3375-2017, 2017.

Gröbner, J.: Example datasets from PMOD/WRC Davos, Switzerland with the double Brewer B163 and QASUME II compared with the UVIOS model. Atmos. Meas. Tech. (supplement comment), 10.5194/amt-2020506-CC1, 2021.

Heikkilä, A., Kaurola, J., Lakkala, K., Karhu, J. M., Kyrö, E., Koskela, T., Engelsen, O., Slaper, H., and Seckmeyer, G.: European UV DataBase (EUVDB) as a repository and quality analyser for solar spectral UV irradiance monitored in Sodankylä, Geosci. Instrum. Method. Data Syst., 5, 333-345, 10.5194/gi-5-333-2016, 2016.

Henderson-Sellers, A., and Wilson, M. F.: Surface albedo data for climatic modeling, Reviews of Geophysics, 21, 1743-1778, https://doi.org/10.1029/RG021i008p01743, 1983.

Henken, C. C., Schmeits, M. J., Deneke, H., and Roebeling, R. A.: Using MSG-SEVIRI Cloud Physical Properties and Weather Radar Observations for the Detection of Cb/TCu Clouds, Journal of Applied Meteorology and Climatology, 50, 1587-1600, 2011.

Herman, J. R.: Global increase in UV irradiance during the past 30 years (1979–2008) estimated from satellite data, Journal of Geophysical Research: Atmospheres, 115, 10.1029/2009jd012219, 2010.

Holick, M. F.: Vitamin D: the underappreciated D-lightful hormone that is important for skeletal and cellular health, Current Opinion in Endocrinology, Diabetes and Obesity, 9, 2002.

Hülsen, G., Gröbner, J., Bais, A., Blumthaler, M., Disterhoft, P., Johnsen, B., Lantz, K. O., Meleti, C., Schreder, J., Vilaplana Guerrero, J. M., and Ylianttila, L.: Intercomparison of erythemal broadband radiometers calibrated by seven UV calibration facilities in Europe and the USA, Atmos. Chem. Phys., 8, 4865-4875, 10.5194/acp-8-4865-2008, 2008.

Hülsen, G., Gröbner, J., Nevas, S., Sperfeld, P., Egli, L., Porrovecchio, G., and Smid, M.: Traceability of solar UV measurements using the Qasume reference spectroradiometer, Applied Optics, 55, 7265 - 7275, 10.1364/AO.55.007265, 2016.

Hülsen, G., Gröbner, J., Bais, A., Blumthaler, M., Diemoz, H., Bolsee, D., Rodríguez, A. D., Fountoulakis, I., Naranen, E., Schreder, J., Stefania, F., and Vilaplana Guerrero, J. M.: Second solar ultraviolet radiometer comparison campaign UVC-II, Metrologia, 2020.

Juzeniene, A., Brekke, P., Dahlback, A., Andersson-Engels, S., Reichrath, J., Moan, K., Holick, M. F., Grant, W. B., and Moan, J.: Solar radiation and human health, Reports on Progress in Physics, 74, 066701, 10.1088/0034-4885/74/6/066701, 2011.

Kato, S., and Marshak, A.: Solar zenith and viewing geometry-dependent errors in satellite retrieved cloud optical thickness: Marine stratocumulus case. Journal of Geophysical Research, 114, D01202, 10.1029/2008JD010579, 2009.

Kazadzis, S., Bais, A., Balis, D., Kouremeti, N., Zempila, M., Arola, A., Giannakaki, E., Amiridis, V., and Kazantzidis, A.: Spatial and temporal UV irradiance and aerosol variability within the area of an OMI satellite pixel, Atmos. Chem. Phys., 9, 4593-4601, 10.5194/acp-9-4593-2009, 2009a.

812 Kazadzis, S., Kouremeti, N., Bais, A., Kazantzidis, A., and Meleti, C.: Aerosol forcing efficiency in the UVA region from
813 spectral solar irradiance measurements at an urban environment, Ann. Geophys., 27, 2515-2522, 10.5194/angeo-27-2515-
814 2009, 2009b.

815 Kazadzis, S., Raptis, P., Kouremeti, N., Amiridis, V., Arola, A., Gerasopoulos, E., and Schuster, G. L.: Aerosol absorption
816 retrieval at ultraviolet wavelengths in a complex environment, Atmos. Meas. Tech., 9, 5997-6011, 10.5194/amt-9-5997-2016,
817 2016.

818 Kerr, J. B., Evans, W. F. J., and Asbridge, I. A.: Recalibration of Dobson Field Spectrophotometers with a Travelling Brewer
819 Spectrophotometer Standard, Atmospheric Ozone, Dordrecht, 1985, 381-386,

820 Kerr, J. B., and Fioletov, V. E.: Surface ultraviolet radiation, Atmosphere-Ocean, 46, 159-184, 10.3137/ao.460108, 2008.

821 Kinne, S.: The MACv2 aerosol climatology, Tellus B: Chemical and Physical Meteorology, 71, 1-21,
822 10.1080/16000889.2019.1623639, 2019.

823 Koren, I., Remer, L. A., Kaufman, Y. J., Rudich, Y., and Martins, J. V.: On the twilight zone between clouds and aerosols,
824 Geophysical Research Letters, 34, https://doi.org/10.1029/2007GL029253, 2007.

825 Kosmopoulos, P. G., Kazadzis, S., Taylor, M., Raptis, P. I., Keramitsoglou, I., Kiranoudis, C., and Bais, A. F.: Assessment of
826 surface solar irradiance derived from real-time modelling techniques and verification with ground-based measurements,
827 Atmos. Meas. Tech., 11, 907-924, 10.5194/amt-11-907-2018, 2018.

828 Kreuter, A., Buras, R., Mayer, B., Webb, A., Kift, R., Bais, A., Kouremeti, N., and Blumthaler, M.: Solar irradiance in the
829 heterogeneous albedo environment of the Arctic coast: measurements and a 3-D model study, Atmos. Chem. Phys., 14, 5989-
830 6002, 10.5194/acp-14-5989-2014, 2014.

831 Krotkov, N. A., Bhartia, P. K., Herman, J. R., Fioletov, V., and Kerr, J.: Satellite estimation of spectral surface UV irradiance
832 in the presence of tropospheric aerosols: 1. Cloud-free case, Journal of Geophysical Research: Atmospheres, 103, 8779-8793,
833 https://doi.org/10.1029/98JD00233, 1998.

834 Lacaze, R., Smets, B., Trigo, I., Calvet, J.C., Jann, A., Camacho, F., Baret, F., Kidd, R., Defourny, P., Tansey, K., et al.: The
835 Copernicus Global Land Service: Present and future. In Proceedings of the EGU General Assembly, Vienna, Austria, 7-12
836 April, 2013.

837 Lakkala, K., Arola, A., Heikkilä, A., Kaurola, J., Koskela, T., Kyrö, E., Lindfors, A., Meinander, O., Tanskanen, A., Gröbner,
838 J., and Hülsen, G.: Quality assurance of the Brewer spectral UV measurements in Finland, Atmos. Chem. Phys., 8, 3369-3383,
839 10.5194/acp-8-3369-2008, 2008.

840 Lakkala, K., Redondas, A., Meinander, O., Thölix, L., Hamari, B., Almansa, A. F., Carreno, V., García, R. D., Torres, C.,
841 Deferrari, G., Ochoa, H., Bernhard, G., Sanchez, R., and de Leeuw, G.: UV measurements at Marambio and Ushuaia during
842 2000–2010, Atmos. Chem. Phys., 18, 16019-16031, 10.5194/acp-18-16019-2018, 2018.

843 Lakkala, K., Kujanpää, J., Brogniez, C., Henriot, N., Arola, A., Aun, M., Auriol, F., Bais, A. F., Bernhard, G., De Bock, V.,
844 Catalfamo, M., Deroo, C., Diémoz, H., Egli, L., Forestier, J. B., Fountoulakis, I., Garcia, R. D., Gröbner, J., Hassinen, S.,
845 Heikkilä, A., Henderson, S., Hülsen, G., Johnsen, B., Kalakoski, N., Karanikolas, A., Karppinen, T., Lamy, K., León-Luis, S.
846 F., Lindfors, A. V., Metzger, J. M., Minvielle, F., Muskatel, H. B., Portafaix, T., Redondas, A., Sanchez, R., Siani, A. M.,
847 Svendby, T., and Tamminen, J.: Validation of TROPOMI Surface UV Radiation Product, Atmos. Meas. Tech. Discuss., 2020,
848 1-37, 10.5194/amt-2020-121, 2020.

849 Larkin, A., Haigh, J. D., and Djavidnia, S.: The Effect of Solar UV Irradiance Variations on the Earth's Atmosphere, Space
850 Science Reviews, 94, 199-214, 10.1023/a:1026771307057, 2000.

851 Levelt, P. F., Oord, G. H. J. v. d., Dobber, M. R., Malkki, A., Huib, V., Johan de, V., Stammes, P., Lundell, J. O. V., and Saari,
852 H.: The ozone monitoring instrument, IEEE Transactions on Geoscience and Remote Sensing, 44, 1093-1101,
853 10.1109/tgrs.2006.872333, 2006.

854 Levelt, P. F., Joiner, J., Tamminen, J., Veefkind, J. P., Bhartia, P. K., Stein Zweers, D. C., Duncan, B. N., Streets, D. G., Eskes,
855 H., van der A, R., McLinden, C., Fioletov, V., Carn, S., de Laat, J., DeLand, M., Marchenko, S., McPeters, R., Ziemke, J., Fu,
856 D., Liu, X., Pickering, K., Apituley, A., González Abad, G., Arola, A., Boersma, F., Chan Miller, C., Chance, K., de Graaf,
857 M., Hakkarainen, J., Hassinen, S., Ialongo, I., Kleipool, Q., Krotkov, N., Li, C., Lamsal, L., Newman, P., Nowlan, C.,
858 Suleiman, R., Tilstra, L. G., Torres, O., Wang, H., and Wargan, K.: The Ozone Monitoring Instrument: overview of 14 years
859 in space, Atmos. Chem. Phys., 18, 5699-5745, 10.5194/acp-18-5699-2018, 2018.

860 López-Solano, J., Redondas, A., Carlund, T., Rodriguez-Franco, J. J., Diémoz, H., León-Luis, S. F., Hernández-Cruz, B.,
861 Guirado-Fuentes, C., Kouremeti, N., Gröbner, J., Kazadzis, S., Carreño, V., Berjón, A., Santana-Díaz, D., Rodríguez-Valido,
862 M., De Bock, V., Moreta, J. R., Rimmer, J., Smedley, A. R. D., Boulkelia, L., Jepsen, N., Eriksen, P., Bais, A. F., Shirotov,
863 V., Vilaplana, J. M., Wilson, K. M., and Karppinen, T.: Aerosol optical depth in the European Brewer Network, Atmos. Chem.
864 Phys., 18, 3885-3902, 10.5194/acp-18-3885-2018, 2018.

865 Lucas, R., McMichael, T., Smith, W., Armstrong, B. K., Prüss-Üstün, A., and World Health, O.: Solar ultraviolet radiation :
866 global burden of disease from solar ultraviolet radiation / Robyn Lucas ... [et al.] ; editors, Annette Prüss-Üstün ... [et al.].
867 Environmental burden of disease series ; no. 13, World Health Organization, Geneva, 2006.

868 Lucas, R. M., Byrne, S. N., Correale, J., Ilschner, S., and Hart, P. H.: Ultraviolet radiation, vitamin D and multiple sclerosis,
869 Neurodegenerative Disease Management, 5, 413-424, 10.2217/nmt.15.33, 2015.

870 Madronich, S.: Environmental UV Photobiology, Environ. UV Photobiol., 10.1007/978-1-4899-2406-3, 1993.

871 Mayer, B., Kylling, A., Madronich, S., and Seckmeyer, G.: Enhanced absorption of UV radiation due to multiple scattering in
872 clouds: Experimental evidence and theoretical explanation, Journal of Geophysical Research: Atmospheres, 103, 31241-
873 31254, https://doi.org/10.1029/98JD02676, 1998.

874 Mayer, B., and Kylling, A.: Technical note: The libRadtran software package for radiative transfer calculations - description
875 and examples of use, Atmos. Chem. Phys., 5, 1855-1877, 10.5194/acp-5-1855-2005, 2005.

876 McKenzie, R., Bernhard, G., Liley, B., Disterhoft, P., Rhodes, S., Bais, A., Morgenstern, O., Newman, P., Oman, L., Brogniez,
877 C., and Simic, S.: Success of Montreal Protocol Demonstrated by Comparing High-Quality UV Measurements with "World
878 Avoided" Calculations from Two Chemistry-Climate Models, Scientific Reports, 9, 12332, 10.1038/s41598-019-48625-z,
879 2019.

880 McKenzie, R. L., Aucamp, P. J., Bais, A. F., Björn, L. O., Ilyas, M., and Madronich, S.: Ozone depletion and climate change:
881 impacts on UV radiation, Photochemical & Photobiological Sciences, 10, 182-198, 10.1039/c0pp90034f, 2011.

882 Meinander, O., Kazadzis, S., Arola, A., Riihelä, A., Räisänen, P., Kivi, R., Kontu, A., Kouznetsov, R., Sofiev, M., Svensson,
883 J., Suokanerva, H., Aaltonen, V., Manninen, T., Roujean, J. L., and Hautecoeur, O.: Spectral albedo of seasonal snow during
884 intensive melt period at Sodankylä, beyond the Arctic Circle, Atmos. Chem. Phys., 13, 3793-3810, 10.5194/acp-13-3793-
885 2013, 2013.

886 MétéoFrance: Algorithm theoretical basis document for cloud products (CMa-PGE01 v3.2, CT-PGE02 v2.2 & CTTH-PGE03
887 v2.2), Technical Report SAF/NWC/CDOP/MFL/SCI/ATBD/01, Paris: MétéoFrance, 2013.

888 Mok, J., Krotkov, N. A., Torres, O., Jethva, H., Li, Z., Kim, J., Koo, J. H., Go, S., Irie, H., Labow, G., Eck, T. F., Holben, B.
889 N., Herman, J., Loughman, R. P., Spinei, E., Lee, S. S., Khatri, P., and Campanelli, M.: Comparisons of spectral aerosol single
890 scattering albedo in Seoul, South Korea, Atmos. Meas. Tech., 11, 2295-2311, 10.5194/amt-11-2295-2018, 2018.

891 Myhre, G., and Myhre, A.: Uncertainties in Radiative Forcing due to Surface Albedo Changes Caused by Land-Use Changes,
892 Journal of Climate, 16, 1511-1524, 10.1175/1520-0442(2003)016<1511:uirfdt>2.0.co;2, 2003.

893 NOAA: Data Announcement 88-MGG-02, Digital relief of the surface of the Earth. NOAA, National Geopgysical Data Center,
894 Boulder, Colorado, 1988.

895 Noël, S., Mieruch, S., Bovensmann, H., and Burrows, J. P.: Preliminary results of GOME-2 water vapour retrievals and first
896 applications in polar regions, Atmos. Chem. Phys., 8, 1519-1529, 10.5194/acp-8-1519-2008, 2008.

897 Peeters, P., Simon, P. C., Hansen, G., Meerkoetter, R., Verdebout, J., Seckmeyer, G., Taalas, P., and Slaper, H.: MAUVE: A
898 European Initiative for Developing and Improving Satellite Derived Ultraviolet Maps, Radiation Protection Dosimetry, 91,
899 201-202, 10.1093/oxfordjournals.rpd.a033200, 2000.

900 Pfeifroth, U., Kothe, S., and Trentmann, J.: Validation report: Meteosat solar surface radiation and effective cloud albedo
901 climate data record (Sarah 2), EUMETSAT SAF CM Validation report with reference number SAF/CM/DWD/VAL/
902 METEOSAT/HEL, 2.1, https://doi.org/10.5676/EUM_SAF_CM/SARAH/V002, 2016.

903 Probst, P., Rizzi, R., Tosi, E., Lucarini, V., and Maestri, T.: Total cloud cover from satellite observations and climate models,
904 Atmospheric Research, 107, 161-170, https://doi.org/10.1016/j.atmosres.2012.01.005, 2012.

905 Raptis, I.-P., Kazadzis, S., Eleftheratos, K., Amiridis, V., and Fountoulakis, I.: Single Scattering Albedo's Spectral Dependence
906 Effect on UV Irradiance., Atmosphere, 9, 10.3390/atmos9090364, 2018.

907 Reda, I., and Andreas, A.: Solar position algorithm for solar radiation applications. NREL Technical Report, NREL/TP-560-
908 34302, Prepared under Task No. WU1D5600, 2008.

909 Renaud, A., Staehelin, J., Fröhlich, C., Philipona, R., and Heimo, A.: Influence of snow and clouds on erythemal UV radiation:
910 Analysis of Swiss measurements and comparison with models, Journal of Geophysical Research: Atmospheres, 105, 4961-
911 4969, https://doi.org/10.1029/1999JD900160, 2000.

912 Rimmer, J. S., Redondas, A., and Karppinen, T.: EuBrewNet – A European Brewer network (COST Action ES1207), an
913 overview, Atmos. Chem. Phys., 18, 10347-10353, 10.5194/acp-18-10347-2018, 2018.

914 Schmalwieser, A., and Siani, A.: Review on Non-Occupational Personal Solar UV Exposure Measurements, Photochemistry
915 and Photobiology, 94, 10.1111/php.12946, 2018.

916 Schmalwieser, A. W., Gröbner, J., Blumthaler, M., Klotz, B., De Backer, H., Bolsée, D., Werner, R., Tomsic, D., Metelka, L.,
917 Eriksen, P., Jepsen, N., Aun, M., Heikkilä, A., Duprat, T., Sandmann, H., Weiss, T., Bais, A., Toth, Z., Siani, A.-M., Vaccaro,
918 L., Diémoz, H., Grifoni, D., Zipoli, G., Lorenzetto, G., Petkov, B. H., di Sarra, A. G., Massen, F., Yousif, C., Aculinin, A. A.,
919 den Outer, P., Svendby, T., Dahlback, A., Johnsen, B., Biszczuk-Jakubowska, J., Krzyscin, J., Henriques, D., Chubarova, N.,
920 Kolarž, P., Mijatovic, Z., Groselj, D., Pribullova, A., Gonzales, J. R. M., Bilbao, J., Guerrero, J. M. V., Serrano, A., Andersson,
921 S., Vuilleumier, L., Webb, A., and O'Hagan, J.: UV Index monitoring in Europe, Photochemical & Photobiological Sciences,
922 16, 1349-1370, 10.1039/c7pp00178a, 2017.

923 Schmalwieser, A. W.: Possibilities to estimate the personal UV radiation exposure from ambient UV radiation measurements,
924 Photochemical & Photobiological Sciences, 19, 1249-1261, 10.1039/d0pp00182a, 2020.

925 Seckmeyer, G., Erb, R., and Albold, A.: Transmittance of a cloud is wavelength-dependent in the UV-range, Geophysical
926 Research Letters, 23, 2753-2755, https://doi.org/10.1029/96GL02614, 1996.

927 Seckmeyer, G., Pissulla, D., Glandorf, M., Henriques, D., Johnsen, B., Webb, A., Siani, A.-M., Bais, A., Kjeldstad, B.,
928 Brogniez, C., Lenoble, J., Gardiner, B., Kirsch, P., Koskela, T., Kaurola, J., Uhlmann, B., Slaper, H., Den Outer, P., Janouch,
929 M., Werle, P., Gröbner, J., Mayer, B., De La Casiniere, A., Simic, S., and Carvalho, F.: Variability of UV Irradiance in Europe,
930 Photochemistry and Photobiology, 84, 172-179, 10.1111/j.1751-1097.2007.00216.x, 2008.

931 Siani, A. M., Casale, G. R., Diémoz, H., Agnesod, G., Kimlin, M. G., Lang, C. A., and Colosimo, A.: Personal UV exposure
932 in high albedo alpine sites, Atmos. Chem. Phys., 8, 3749-3760, 10.5194/acp-8-3749-2008, 2008.

933 Slaper, H., Reinen, H. A. J. M., Blumthaler, M., Huber, M., and Kuik, F.: Comparing ground-level spectrally resolved solar
934 UV measurements using various instruments: A technique resolving effects of wavelength shift and slit width, Geophysical
935 Research Letters, 22, 2721-2724, 10.1029/95gl02824, 1995.

936 Smedley, A. R. D., Rimmer, J. S., Moore, D., Toumi, R., and Webb, A. R.: Total ozone and surface UV trends in the United
937 Kingdom: 1979–2008, International Journal of Climatology, 32, 338-346, 10.1002/joc.2275, 2012.

938 Svendby, T., Hansen, G. H., Bäcklund, A., and Dahlback, A.: Monitoring of the atmospheric ozone layer and natural ultraviolet
939 radiation: Annual report 2018, NILU M-1462 | 2019, 39, 2018.

940 Taylor, M., Kosmopoulos, P. G., Kazadzis, S., Keramitsoglou, I., and Kiranoudis, C. T.: Neural network radiative transfer
941 solvers for the generation of high resolution solar irradiance spectra parameterized by cloud and aerosol parameters, Journal
942 of Quantitative Spectroscopy and Radiative Transfer, 168, 176-192, https://doi.org/10.1016/j.jqsrt.2015.08.018, 2016.

943 Vanicek, K., Frei, T., Litynska, Z., and Schmalwieser, A.: UV-Index for the Public, European Union, 2000.

944 Verdebout, J.: Amethod to generate surface UV radiation maps over Europe using GOME, Meteosat and ancillary geophysical
945 data. Journal of Geophysical Research: Atmospheres, 105(D4), 5049-5058, 2000.

946 Verdebout, J.: A Satellite-Derived UV Radiation Climatology over Europe to Support Impact Studies, Arctic, Antarctic, and
947 Alpine Research, 36, 357-363, 10.1657/1523-0430(2004)036[0357:asurco]2.0.co;2, 2004.

948 Vitt, R., Laschewski, G., Bais, A. F., Diémoz, H., Fountoulakis, I., Siani, A.-M., and Matzarakis, A.: UV-Index Climatology
949 for Europe Based on Satellite Data, Atmosphere, 11, 10.3390/atmos11070727, 2020.

950 Webb, A. R., and Engelsen, O.: Ultraviolet Exposure Scenarios: Risks of Erythema from Recommendations on Cutaneous
951 Vitamin D Synthesis, in: Sunlight, Vitamin D and Skin Cancer, edited by: Reichrath, J., Springer New York, New York, NY,
952 72-85, 2008.

953 Webb, A. R., Slaper, H., Koepke, P., and Schmalwieser, A. W.: Know Your Standard: Clarifying the CIE Erythema Action
954 Spectrum, Photochemistry and Photobiology, 87, 483-486, 10.1111/j.1751-1097.2010.00871.x, 2011.

955 WHO: Global Solar UV Index: A Pratical Guide, No. WHO/SD., Geneva, Switzerland, 2002.

956 WMO: Report of the WMO Meeting of Experts on UVB Measurements, Data Quality and Standardization of UV Indices,
957 1994, 1995.

958 Zempila, M.-M., Koukouli, M.-E., Bais, A., Fountoulakis, I., Arola, A., Kouremeti, N., and Balis, D.: OMI/Aura UV product
959 validation using NILU-UV ground-based measurements in Thessaloniki, Greece, Atmospheric Environment, 140, 283-297,
960 https://doi.org/10.1016/j.atmosenv.2016.06.009, 2016.

961 Zerefos, C. S., Tourpali, K., Eleftheratos, K., Kazadzis, S., Meleti, C., Feister, U., Koskela, T., and Heikkilä, A.: Evidence of
962 a possible turning point in solar UV-B over Canada, Europe and Japan, Atmos. Chem. Phys., 12, 2469-2477, 10.5194/acp-12-
963 2469-2012, 2012.

964

965

966

967

968

969

970

971

972

973

974

975

976

977

978
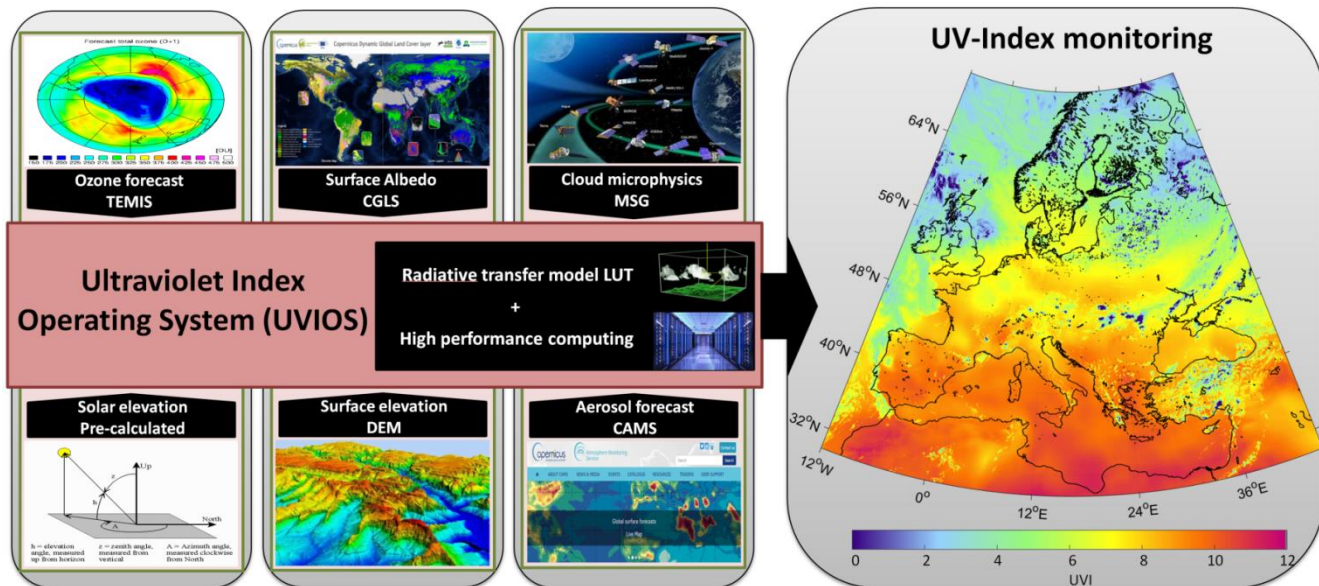
979

980
981
982
983
984
985
986
987
988
989
990

Table 1: UVIOS model input parameters

Parameter	Description (spatial – temporal resolution)	Source	Reference
Cloud microphysics	Nowcast cloud optical thickness (COT), cloud phase (CPH) (5 km – 15 minutes)	Meteosat Second Generation (MSG4) NOA Antenna	(MétéoFrance, 2013)
Aerosol optical depth	1-day forecast aerosol optical depth (AOD) (40 km – 3 hours)	Copernicus Atmosphere Monitoring Service (CAMS) – FTP access	(Eskes et al., 2015)
Aerosol optical properties	Single scattering albedo (SSA), Angstrom exponent (AE) (1 x 1 degrees – 1 month)	Aerosol Comparisons between Observations and Models (Aerocom)	(Kinne, 2019)
Solar elevation	Solar zenith angle (SZA) (5 km – 15 minutes)	Astronomical model In-house software (NOA)	(Reda and Andreas, 2008)
Surface albedo	Surface albedo (ALB) (1 km – 12 days)	Copernicus Global Land Service (CGLS)	(Carrer et al., 2010)
Water vapor	H_2O observation (40 x 80 km – 1day)	Global Ozone Monitoring Experiment 2 Level 2 data (GOME-2 L2)	(Noël et al., 2008)
Surface elevation	Elevation observation (ELE) (1 m – fixed)	Digital Elevation Model (DEM) In-house database (NOAA)	(NOAA, 1988)
Ozone	1-day forecast total ozone column (TOC) (1 x 1 degrees – 1 day)	Tropospheric Emission Monitoring Internet Service (TEMIS) with Assimilated Ozone Fields from GOME-2 (METOP-B)	(Eskes et al., 2003)

991
992
993
994
995
996
997
998
999
1000

1001

1002

1003

1004

1005

1006

1007

1008

1009

1010

1011

Figure 1: Flowchart illustration of the UVIOS modelling technique scheme. The pre-calculated effects of solar and surface elevation and albedo followed by the aerosol and ozone forecasts and the real-time cloud observations to the UVIOS solver result in the spectrally weighted output of UVI for the European region.

1015

1016

1017

1018

1019

1020

1021

1022

1023

1024

1025

1026

1027

1028

1029

1030
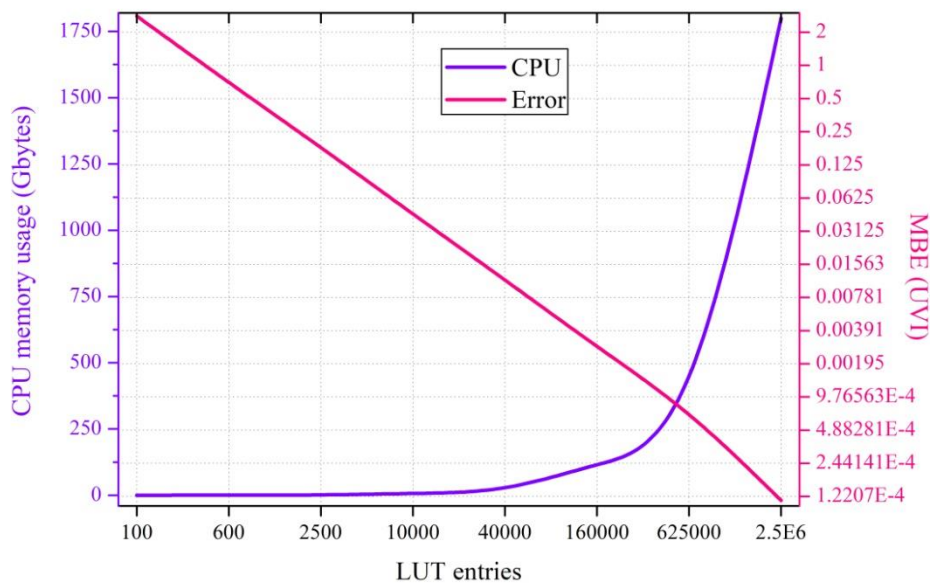
Figure 2: UVIOS memory usage and error statistics in terms of mean bias error (MBE) for a range of different LUT sizes.

1033

1034

1035

1036

1037

1038

1039

1040

1041
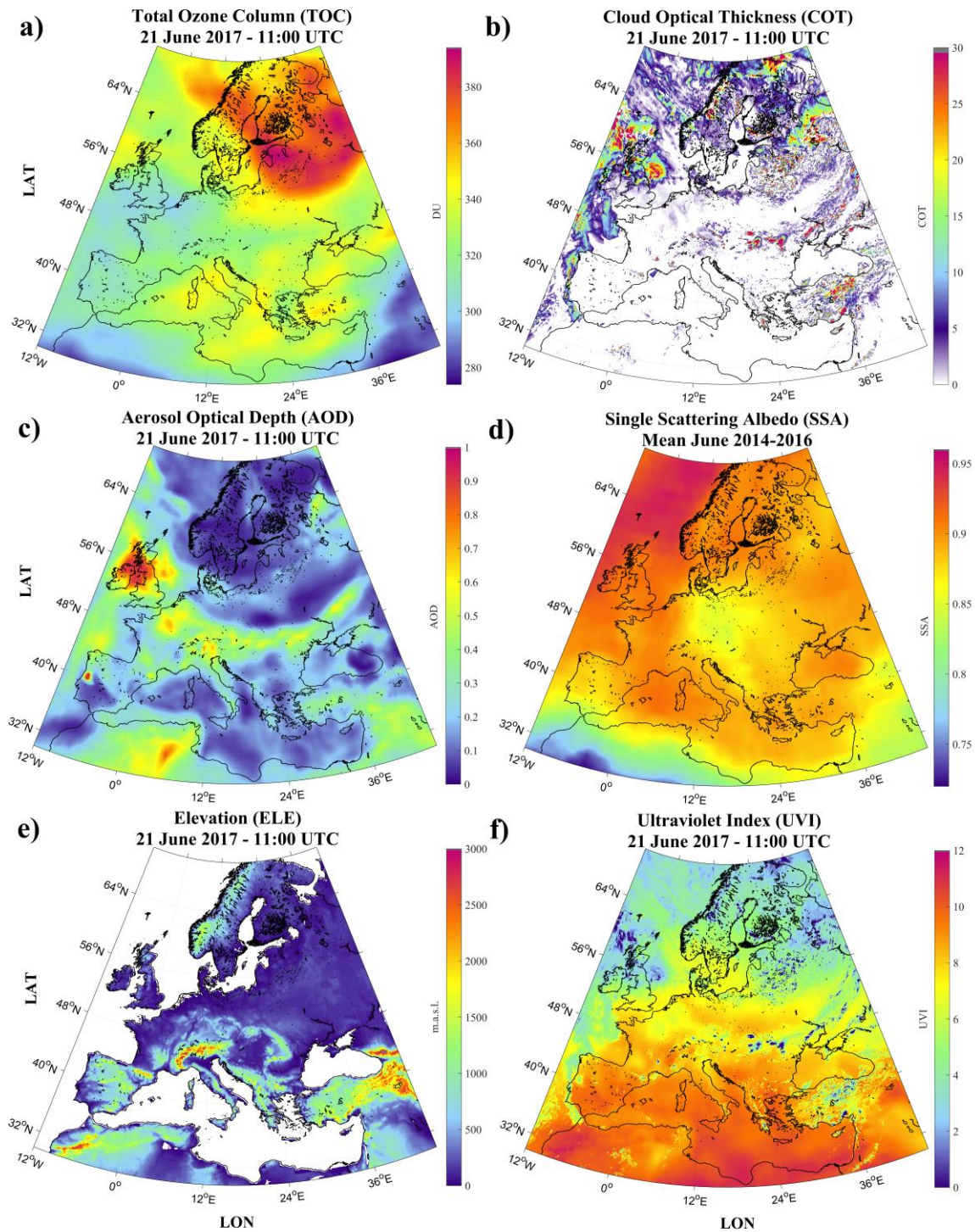
Figure 3: An example of the input TOC (a), COT (b), AOD (c), SSA (d), ELE (e) and output UVI (f) maps based on the UVIOS modelling
technique applied for the 21st of June 2017 at 11:00 UTC.
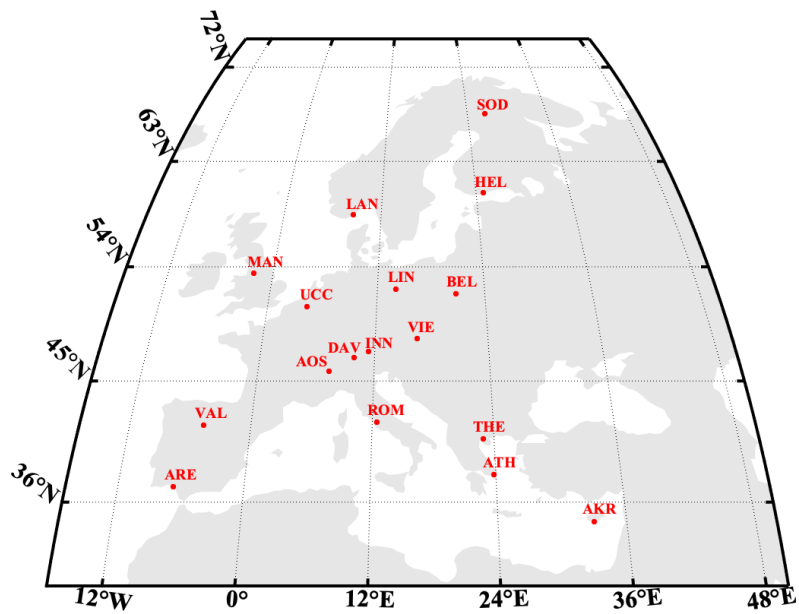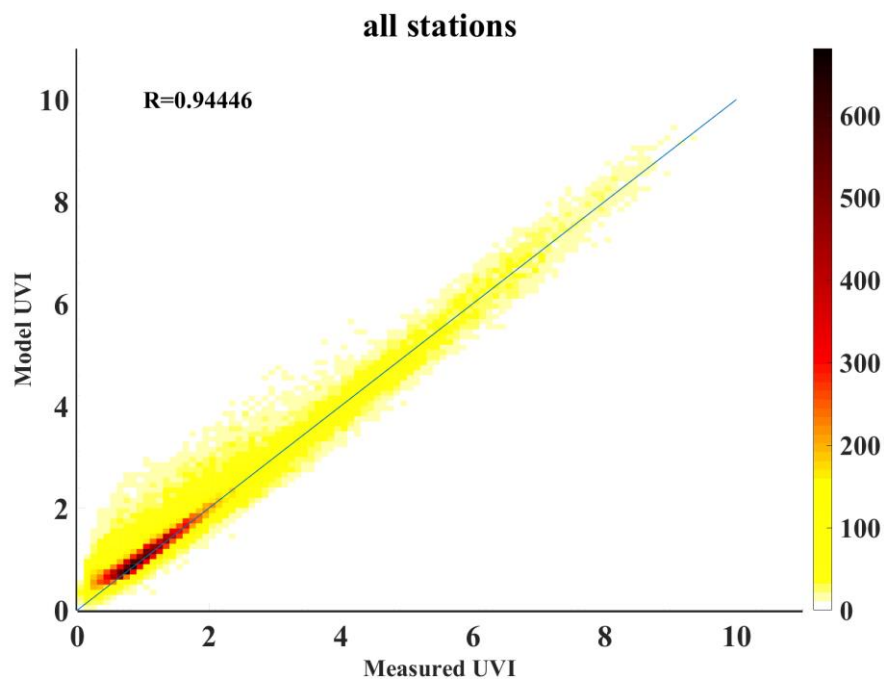
Figure 4: Study region and UVI ground measurement locations.

1066

1067

1068

1069

1070

1071

Table 2: Coordinates (degrees), instrument type, height (metres above sea level) and maximum UVI measured levels of the European stations used for the comparison.
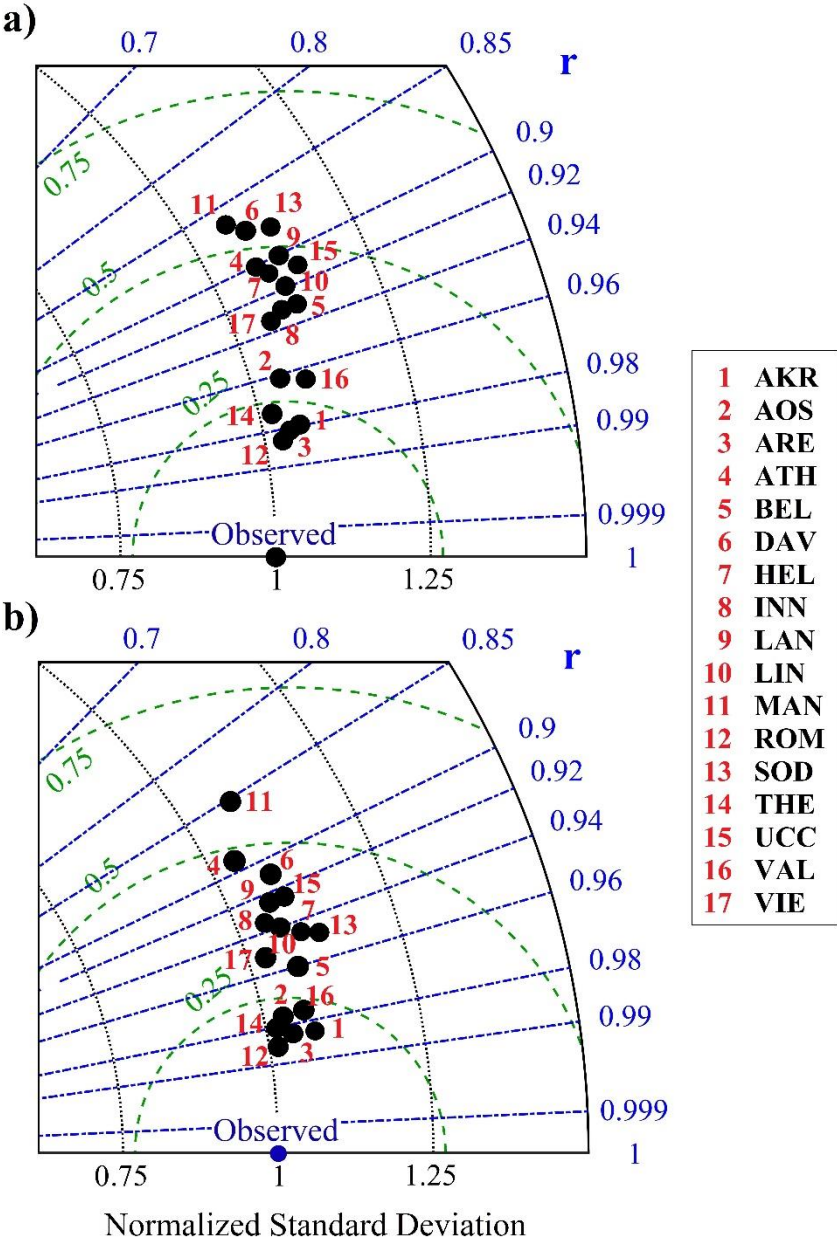
Station	Country	Code	Latitude (ºN)	Longitude (ºE)	Instrument	Height (m.a.s.l.)	UVImax	Reference
Akrotiri	Cyprus	**AKR**	34.59	32.99	SL501	23	9.14	
Aosta	Italy	**AOS**	45.74	7.36	Bentham DTMc300	570	9.60	(Fountoulakis et al., 2020b)
El Arenosillo	Spain	**ARE**	37.10	-6.73	Brewer MKIII	52	9.78	
Athens	Greece	**ATH**	37.99	23.78	Brewer MKIV	180	10.20	
Belsk	Poland	**BEL**	51.84	20.79	Brewer MKIII	176	7.54	(Czerwińska et al., 2016)
Davos	Switzerland	**DAV**	46.81	9.84	Brewer MKIII	1590	10.57	
Helsinki	Finland	**HEL**	60.20	24.96	Brewer MKIII	48	5.68	(Lakkala et al., 2008)
Innsbruck	Austria	**INN**	47.26	11.38	SL501	577	8.35	(Hülsen et al., 2020)
Landvik	Norway	**LAN**	58.33	8.52	GUV-541	10	6.65	(Svendby et al., 2018)
Lindenberg	Germany	**LIN**	52.21	14.11	Bentham DTMc300	127	8.86	
Manchester	United Kingdom	**MAN**	53.47	-2.23	Brewer MKII	76	7.30	(Smedley et al., 2012)
Rome	Italy	**ROM**	41.90	12.50	Brewer MKIV	75	8.38	
Sodankyla	Finland	**SOD**	67.37	26.63	Brewer MKIII	179	4.51	(Heikkilä et al., 2016; Lakkala et al., 2008)
Thessaloniki	Greece	**THE**	40.63	22.96	Brewer MKIII	60	10.40	(Fountoulakis et al., 2016; Garane et al., 2006)
Uccle	Belgium	**UCC**	50.80	4.35	Brewer MKIII	100	8.99	(De Bock et al., 2014)
Valladolid	Spain	**VAL**	41.66	-4.71	YES	705	10.32	(Hülsen et al., 2020)
Vienna	Austria	**VIE**	48.26	16.43	SL501	153	8.09	(Hülsen et al., 2020)

1074

1075

1076

1077

1078

1081
1082
1083
1084
1085
1086
1087
1088

all stations

1089

Figure 56: Scatter plot of the overall UVIOS performance for all stations. The analytical statistics for each station can be found in the Appendix A.

1092

1093

1094

1095

1096

1097

1098

1099

1100

1101

1102

1103

1104 **Figure 65**: Taylor diagram for the overall UVIOS accuracy for all ground-stations under all sky (a) and clear sky (b) conditions.

1105

1106

1107

1108

1109

1110

1111

1112

1113

1114

1115

1116 **Table 3:** Absolute difference between UVIOS~~modelled~~ and ground--based UVI measurements in terms of percentages (%) of data that are
1117 within 0.5 and 1 UVI of difference (U0.5 and U1.0, respectively) as well as the correlation coefficient (r)~~R~~ for all sky and clear sky conditions.

STATION	ALL SKY			CLEAR SKY		
	U0.5	U1.0	r~~R~~	U0.5	U1.0	r~~R~~
AKR	82.25	96.02	0.980	84.57	97.48	0.987
AOS	86.81	94.40	0.961	92.23	97.07	0.978
ARE	85.15	95.73	0.981	87.99	96.86	0.986
ATH	84.99	94.29	0.902	88.98	96.35	0.891
BEL	83.07	93.28	0.933	91.30	96.50	0.960
DAV	74.20	86.43	0.873	76.19	87.06	0.912
HEL	86.53	94.79	0.909	94.13	97.70	0.944
INN	79.96	92.17	0.932	87.09	95.23	0.937
LAN	84.94	93.46	0.900	92.34	96.52	0.925
LIN	81.58	91.86	0.919	90.95	96.31	0.941
MAN	77.72	90.44	0.862	87.85	94.27	0.852
ROM	87.69	96.19	0.985	89.55	97.00	0.991
SOD	90.86	97.26	0.883	95.69	98.94	0.947
THE	88.98	95.91	0.974	92.51	97.35	0.981
UCC	71.18	87.68	0.913	83.23	92.15	0.926
VAL	85.86	93.93	0.962	86.61	95.22	0.976
VIE	76.65	91.53	0.936	83.37	94.42	0.952

1118

1119

1120

1121

1122

1123

1124

1125

1126

1127

1128

1129

1130

1131

1132

1133

1134

1135

1136

1137

1138

1139

1140

1141

1142

1143

Table 4: Mean bias error of the TEMIS TOC as compared to the WOUDC ground-based measurements.

Station	AOS	ATH	DAV	MAN	ROM	SOD	THE	UCC
MBE TOC (DU)	7.6	-0.9	1.9	5.0	-9.9	-5.4	-2.2	2.9
RMSE TOC (DU)	15.8	10.0	9.1	11.3	12.5	13.1	6.2	7.8
rR	0.92	0.95	0.97	0.97	0.94	0.97	0.99	0.98

1144

1145

1146

1147

1148

1149

1150

1151

1152

1153

1154

1155

1156

1157

1158

1159

1160

1161

1162

1163

1164

1165

1166

1167

1168

1169

1170
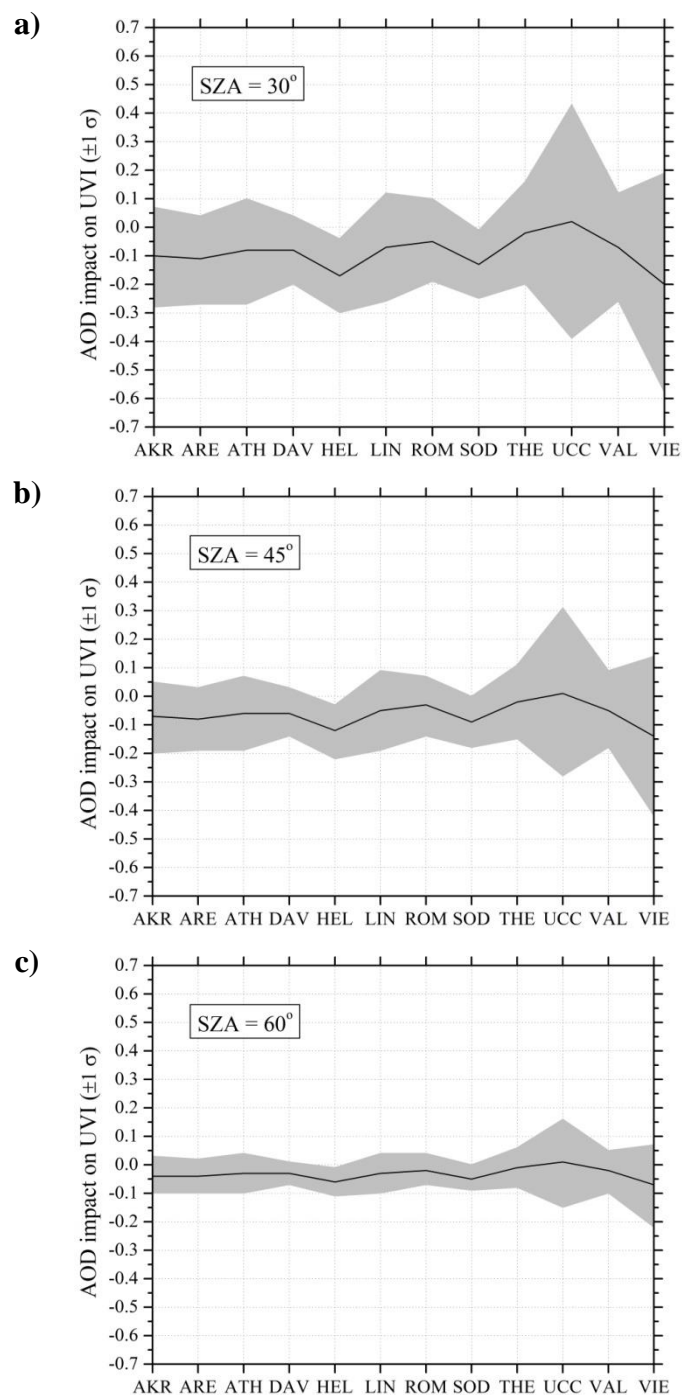
Figure 76: Differences of UVI derived by the UVIOS using as input the TEMIS and the Brewer TOC respectively at all stations with available data. (lower possible SOD SZA is 44 degrees).

1173

1174

1175

1176

1177

1178

1179

1180
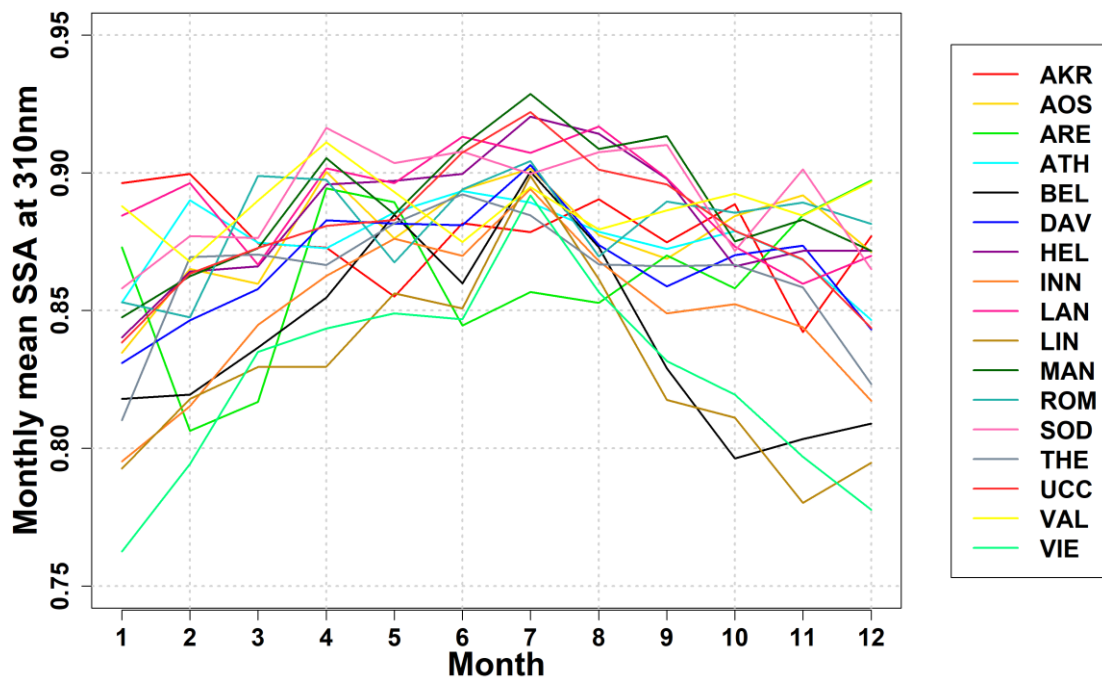
1181
1182
1183
1184
1185
1186
1187
1188
1189
1190
1191
1192
1193
1194
1195

1196 **Table 5:** Comparison results between CAMS forecasted AOD values used as UVIOS input and AERONET ground-based AOD
1197 measurements. The AOD MBE and RMSE statistical scores are shown in absolute units, along with correlation coefficient.

Station	AKR	ARE	ATH	DAV	HEL	LIN	ROM	SOD	THE	UCC	VAL	VIE
MBE	0.037	0.042	0.030	0.029	0.062	0.026	0.017	0.047	0.008	-0.007	0.024	0.071
RMSE	0.074	0.070	0.074	0.053	0.078	0.074	0.056	0.065	0.066	0.150	0.073	0.157
rR	0.77	0.91	0.80	0.73	0.70	0.69	0.80	0.63	0.76	0.50	0.78	0.10

1198
1199
1200
1201
1202
1203
1204
1205
1206
1207
1208
1209
1210

1211
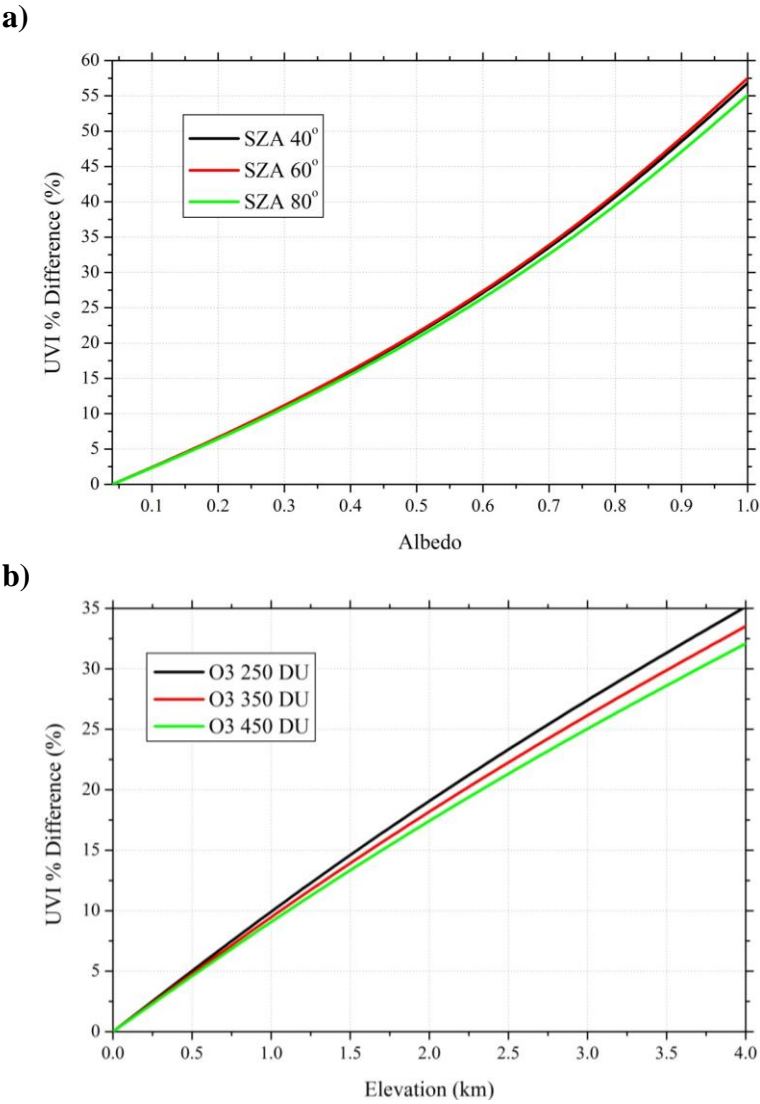
1212 **Figure 87:** The mean bias error of the CAMS – AERONET AOD impact on UVI for all stations with available data as a function of SZA at
1213 30 (a), 45 (b) and 60 (c) degrees together with the uncertainty range (± 1 σ).

1214

1215

1216

1217

1218

1219

1220

1221

1222

1223 **Figure 98:** The monthly mean (i.e. 1-12 = Jan-Dec) SSA levels for all ground stations as derived by the MACv2 database.

1224

1225

1226

1227

1228

1229

1230
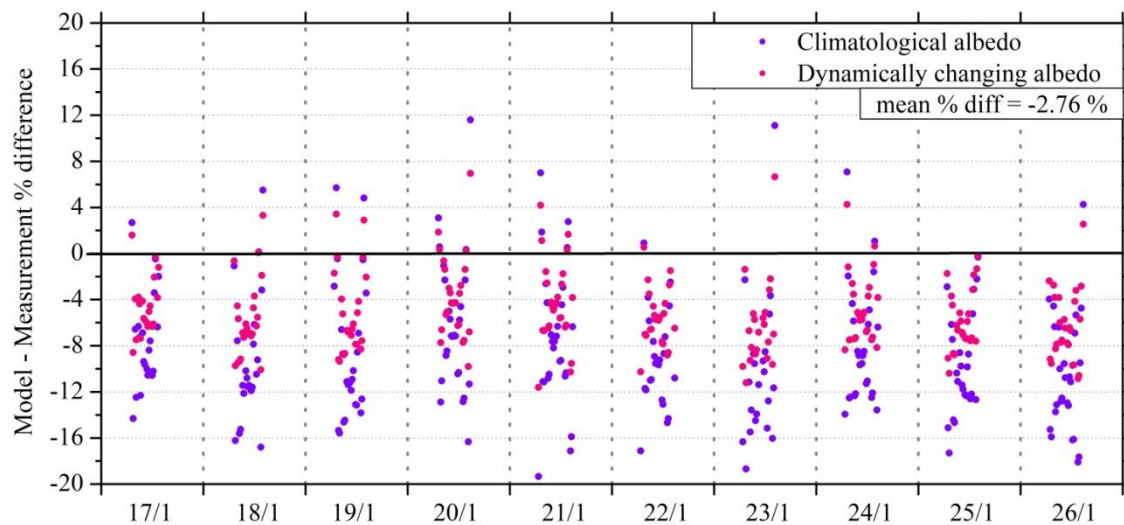
1231

1232

1233

1234

1235

a)

b)
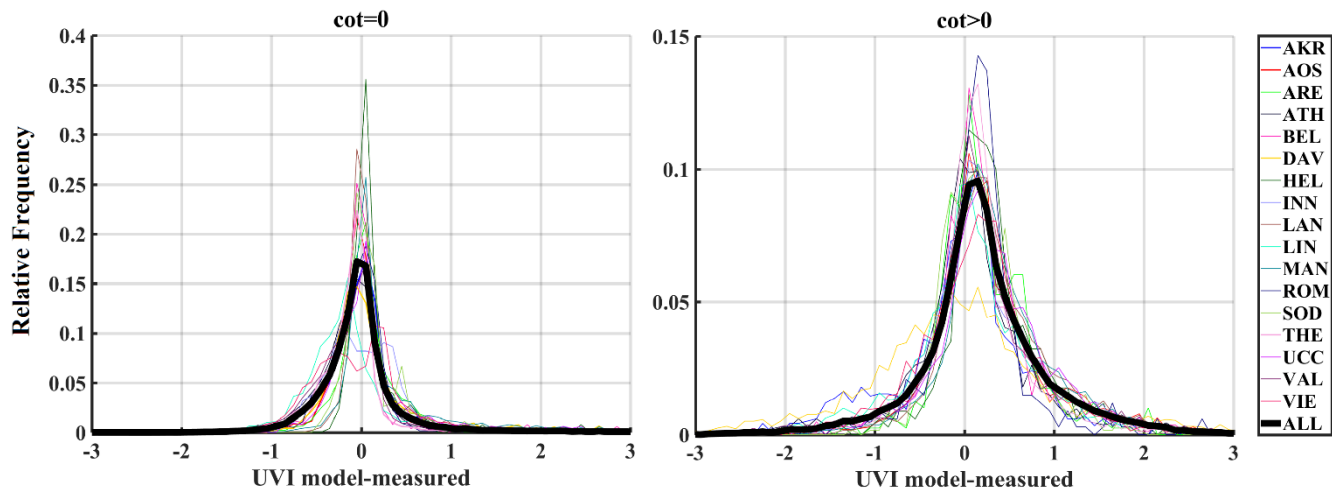
1236

Figure 105: The surface albedo effect on UVI as a function of percentage difference for various SZAs (a). The surface elevation effect on UVI as a function of percentage difference for various total ozone columns (b).

1239

1240

1241

1242

1243

1244

1245

1246

1247

1248

1249

1250

1251

1252

1253
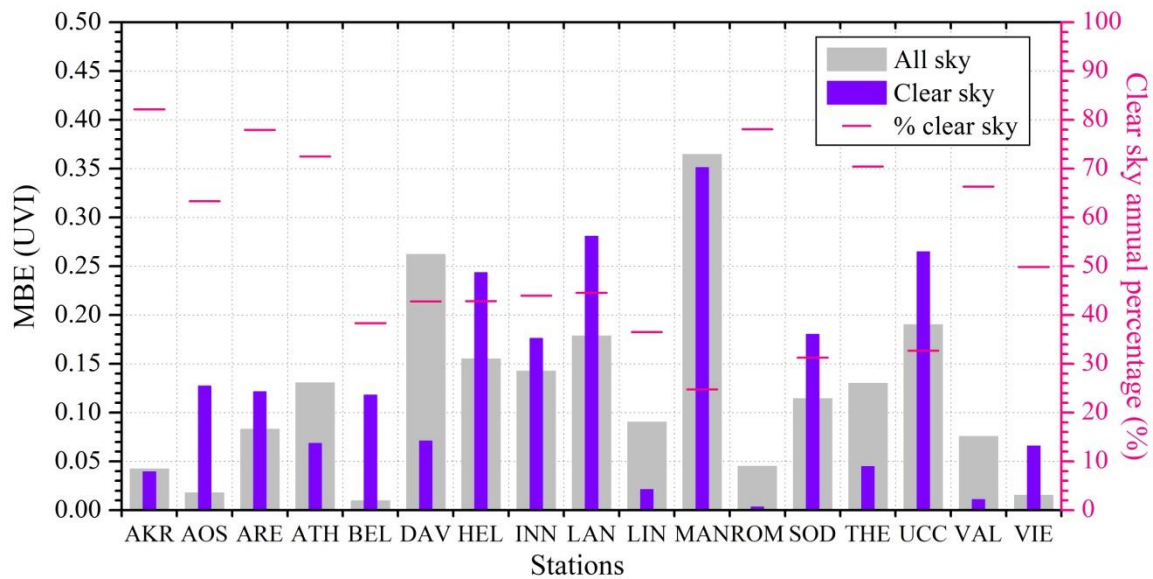
Figure 1~~1~~0: The effect of surface albedo correction on UVI for the Davos station. The climatological and the dynamically changing albedo in terms of percentage differences of modelled and ground measurements during a snow covered period (17/1 - 26/1) under clear sky conditions.

1257

1258

1259

1260

1261

1262

1263

1264

1265
1266
1267
1268
1269
1270
1271
1272
1273
1274
1275
1276

1277

Figure 12~~1~~: Relative frequency distribution of UVI residuals for all stations (coloured lines) and the mean (bold black line) for cloudless (left~~upper~~ plot) and cloudy (right~~lower~~ plot) conditions.

1280
1281
1282
1283
1284
1285
1286
1287

1288

1289

1290

1291

1292

1293

1294

1295

1296

1297

1298

1299

1300
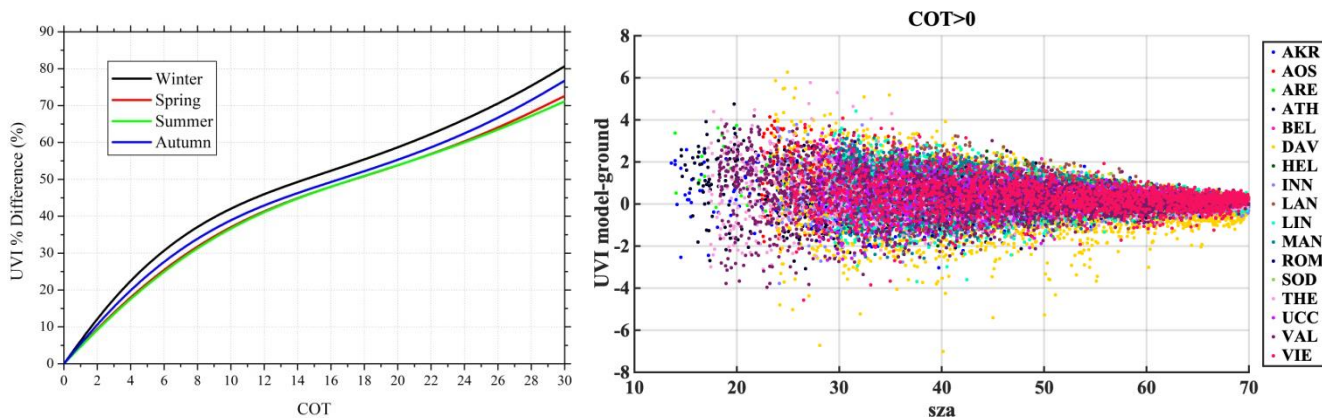
Figure 1~~3~~2: Mean bias error of the modelled UVI as compared to the ground-based measurements for all and clear sky conditions. The percentage of clear sky data time steps was also plotted with red lines.

1303

1304

1305

1306

1307

1308

1309

1310

1311

1312

1313

1314

1315

1316

1317

1318

1319

1320

1321

1322

1323

1324

Table 6: Percentage of data for UVIOS underestimation (A1-A3) and overestimation (B1-B3) under clear and cloudy sky conditions for various UVI difference (modelled-ground) classes.

Difference of UVI	< -1.0 (A1)	< -0.5 (A2)	< 0.0 (A3)	> 0.0 (B3)	> 0.5 (B2)	> 1.0 (B1)
% of data COT > 0	3.6	11.5	37.5	62.5	24.8	11.1
% of data COT = 0	0.9	10.2	45.4	54.6	11.4	4.2

1327

1328

1329

1330

1331

1332

1333

1334

1335

1336

1337

1338

1339

1340
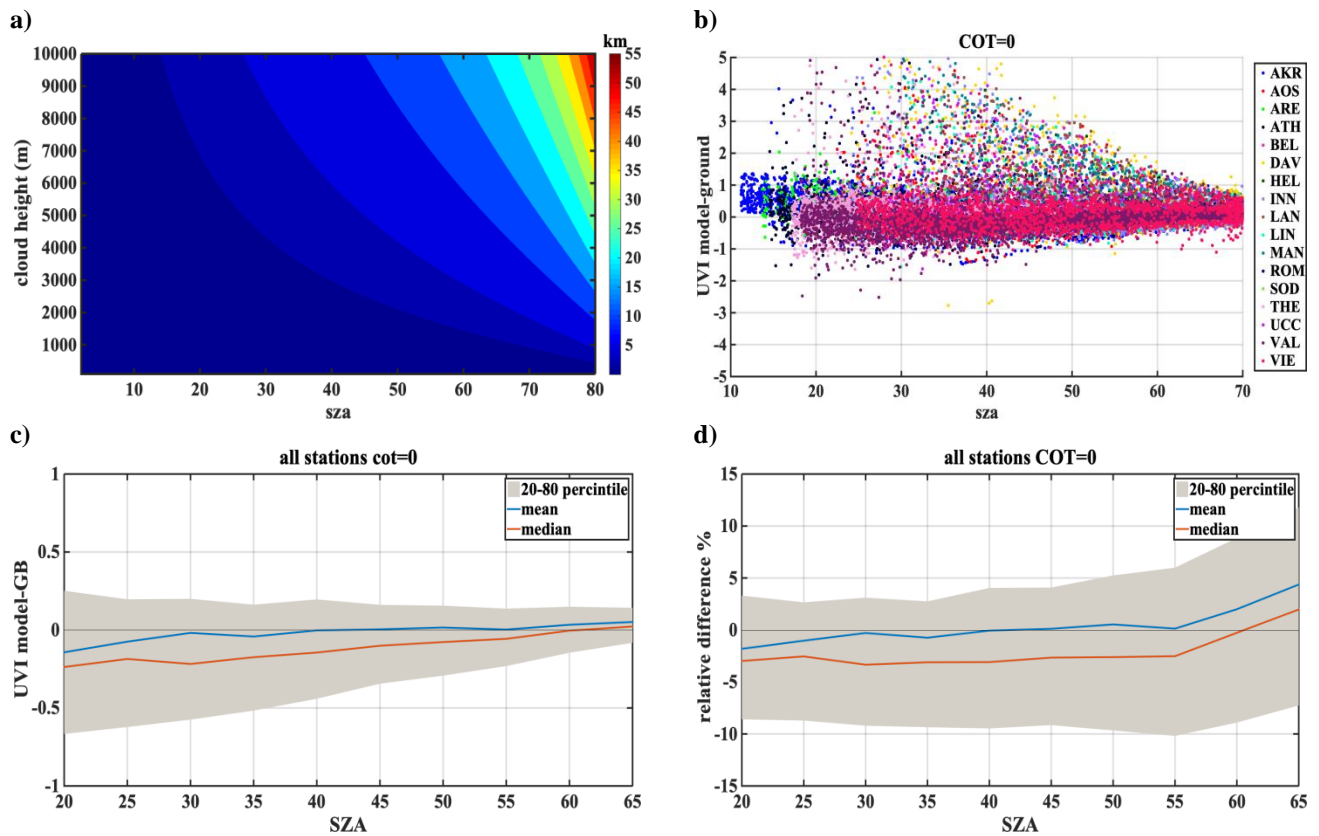
1341

1342

1343

1344

1345

1346

1347

1348

1349

1350

1351

1352

1353

Figure 143: The average COT effect on UVI as a function of percentage difference for all seasons (left) and scatterplot of the UVI difference under cloudy sky conditions for all stations (right).

1354
1355

1356

1357

1358

1359

1360

1361

1362

1363

1364

1365

1366

1367

1368

1369

1370

1371

1372

1373

Figure 1~~5~~4: ~~a).~~ The shadow volume at the surface level of a cloud relative to the SEVIRI angle view, as a function of cloud height and SZA ~~surface distance of the projection of a cloud relative to the instrument in order to block the sun as a function of the cloud height and the SZA~~ (a). ~~(b).~~ Scatterplot of the UVI difference under clear sky conditions for all stations (b). ~~c d)~~ UVI mean, median and 20-80 percentile differences (c) and percentage differences (d) derived by the UVIOS as compared to the ground-based measurements for clear sky conditions as a function of SZA.

1379

1380

1381

Appendix A

The following set of Figures (A.1 – A.17) show for all stations, density scatterplots of measured and modeled UVI for all sky and clear sky conditions (upper row), normalized probability histogram of differences (middle row), and boxplot of differences (lower row) as a function of SZA, representing median (red lines), mean (blue dotted lines) 25-75 percentiles (blue boxes) and 5-95 whiskers (dotted lines).Table A.1 shows additionally the amount of data points that represent both all sky and clear sky conditions for the studied stations.

We have categorized the stations mostly based on cloud cover as Mediterranean, Central Europe, High altitude and High latitude. Each of the station has its own characteristics in terms of atmospheric conditions and parameters affecting the UVI reaching the ground. A summary of the results with possible explanation of the differences observed are shown here. The Mediterranean region includes the stations THE, ATH, AKR, ROM, VAL and ARE. Analysis of TOC showed that in most of the cases UVI mean differences are less than 0.1 in general while a negative bias between TOC and the ground measurements was seen to be highest for ROM (-9.9) that corresponds to the UVI difference of 0.3. Impact of AOD uncertainty showed the correlation coefficient between the modelled and the measured UVI values above 0.7 for most of the stations while it was as high as 0.91 for ARE. The mean bias between the modelled and measured UVI for clear sky condition was found to be less than that for the all sky condition for the stations AKR, ATH and THE that had most days of the year as cloud-free (the clear sky percentage is above 70%). The mean bias between the modelled and measured UVI for clear sky condition was more than the all sky condition for ARE even though it had mostly clear skies throughout the year. The analysis of the combined effect of the aerosol and ozone at Thessaloniki revealed that the model showed a slight underestimation with real inputs (AERONET and Brewer) while overestimations for forecasted inputs (CAMS and TEMIS). However, the coefficient of correlation was found to be as 0.989 and 0.992 for the model with forecasted and real inputs, respectively. Stations of this classification have the single scattering albedo ranging from 0.76 to 0.93, with most of them having SSA values between 0.83 to 0.93 except stations ARE and THE that had relatively smaller SSA values (0.76-0.9) and greater variability, and large MBE. AKR station comparison showed some UVIOS calculated UVI at higher levels than the ground-based~~GB~~ measurements especially in low SZA's. However, ground-based~~GB~~ UVI measurements seem more unrealistic than the UVIOS calculated UVI for summer local noon conditions as modeled UVIs with real AOD and TOC measurements at the area tend to agree with UVIOS outputs. The second classification is the Central European regions including AOS, UCC, BEL, MAN, LIN, VIE and INN. The median of the absolute UVI differences between the model and the measurement for all sky condition were higher for MAN and UCC while for others it was close to zero. Larger UVI difference of -0.22 due to TOC uncertainty impact was observed for AOS which might be due to large values of UVI at higher altitude as the positive bias is highest for AOS station (7.6). The UVIOS MBE and RMSE statistical scores for analyzing AOD uncertainty impact showed a mean positive bias up to 0.071 for all the stations except UCC which is showed a mean negative bias of 0.007. The mean bias between the modelled and measured UVI for clear sky condition was more than the all sky condition for AOS even though it had mostly clear skies throughout the year. BEL, UCC and VIE showed more MBE for clear sky condition than the all sky condition as they have mostly cloudy skies

throughout the year (clear sky annual percentage less than 50%). However, stations LIN and MAN also have more MBE for clear sky condition even though they have most days of the year as cloudy (clear sky annual percentage less than 45%). Analysis of AOD uncertainty showed that UVI difference was highest for VIE than the other stations. The monthly values of the single scattering albedo used in UVIOS ranged from 0.76 to 0.93 for stations AOS, UCC and MAN, with most of them having SSA values between 0.83 to 0.93, and relatively small variability. While, the stations BEL, INN, LIN and VIE had relatively smaller SSA values (0.76-0.9) and greater variability than the other stations and most of these stations have shown large MBE.

The high altitude station is DAV and high latitude stations include LAN, HEL and SOD. DAV have less MBE for clear sky condition even though they have most days of the year as cloudy (clear sky annual percentage less than 45%). DAV and MAN show worse statistical behavior for clear sky, which is probably caused by misclassification of cloudy pixels. For DAV this could be explained by the complex mountainous topography of the area. Large UVI differences in SOD and HEL indicate higher introduced uncertainties over higher latitudes. Higher aerosol levels in the atmosphere tend to lower the UVI. Highest difference in UVI is observed for the stations HEL, SOD and VIE. Since, the aerosol level at the stations HEL and SOD is very low this leads to higher UVI which can be the reason for the small UVI differences observed for these stations. The sStations of this classification have mostly cloudy skies throughout the year (clear sky annual percentage less than 50%) and have more MBE for clear sky condition than the all sky condition. This might be due the fact that the clouds are not captured well at a point station and a cloudy sky might have been considered as a clear sky. Higher UVI difference was observed for HEL and SOD as a result of AOD uncertainty analysis which might be due to the low aerosol content of these stations due to higher latitude that leads to higher UVI values.

Table A.1 Number of data points and clear sky data points, used in the analysis for each station.

Station	All data	Data COT=0
AKR	6547	5379
AOS	5607	3551
ARE	1814	1414
ATH	4892	3548
BEL	1317	505
DAV	5635	2410
HEL	595	255
INN	4365	1919
LAN	7409	3302
LIN	3795	1387
MAN	7854	1946
ROM	1532	1196
SOD	860	269
THE	9750	6867
UCC	3007	983
VAL	9795	6497
VIE	4199	2094
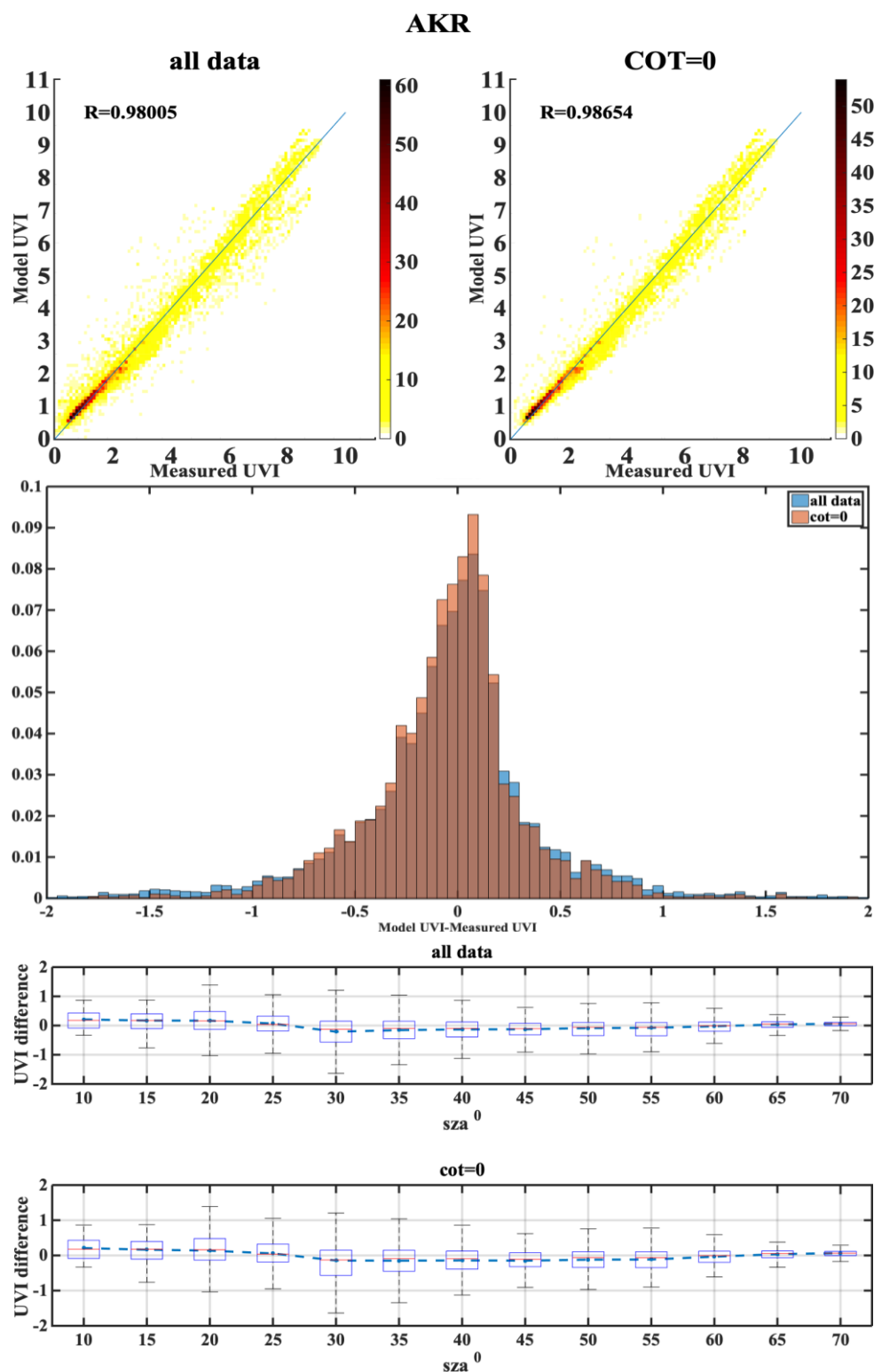
Figure A.1
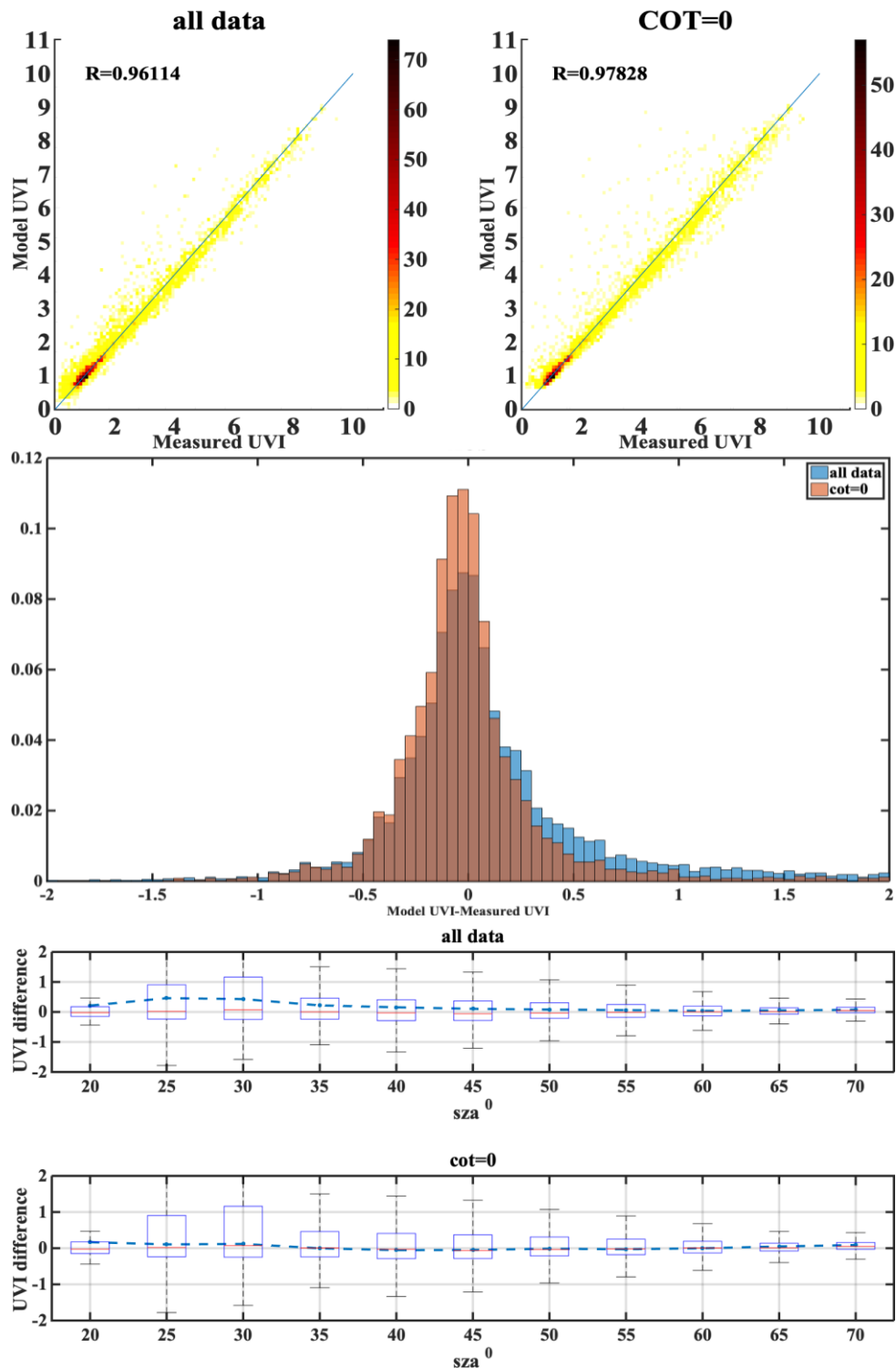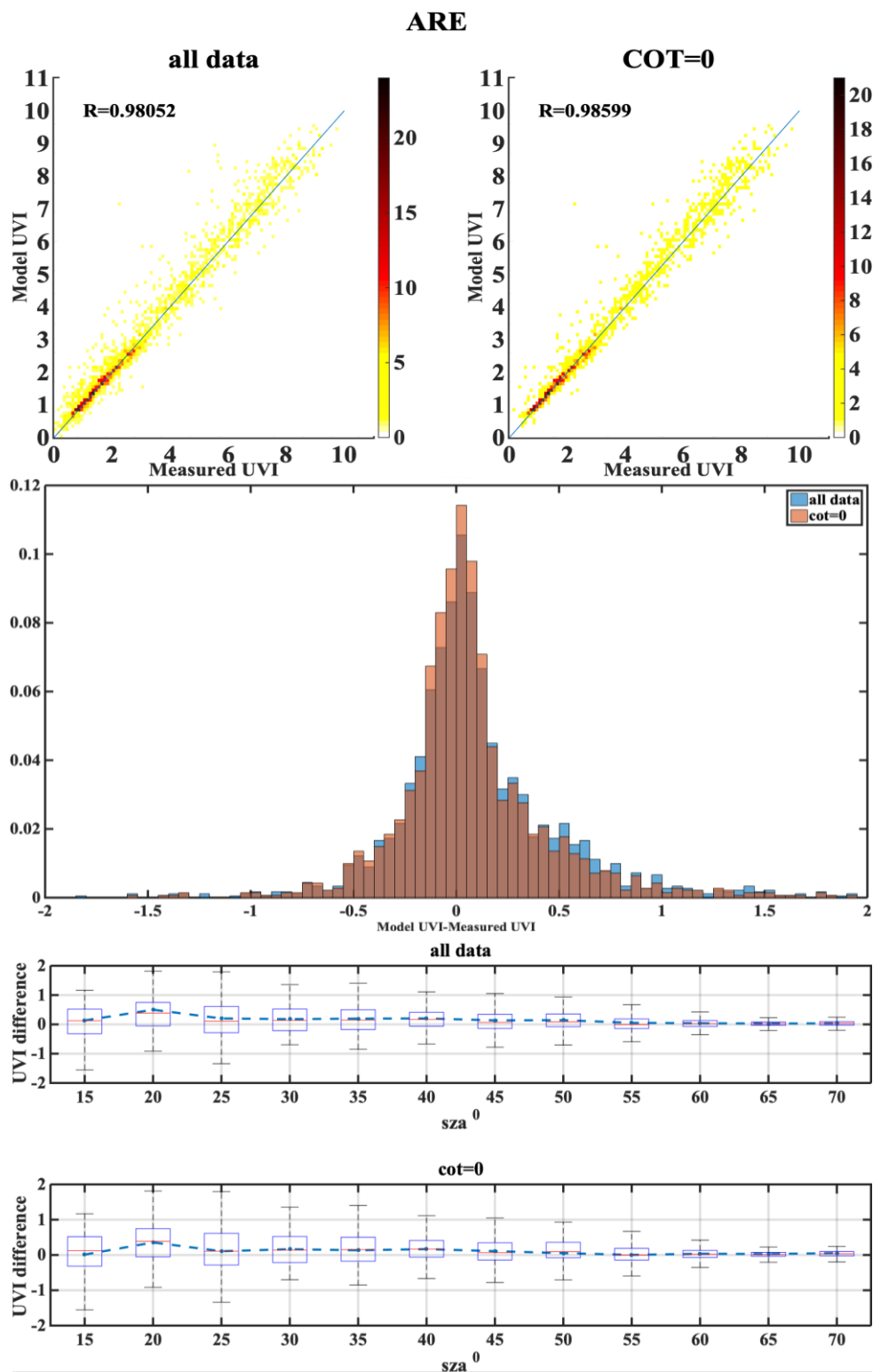
Figure A.2

Figure A.3
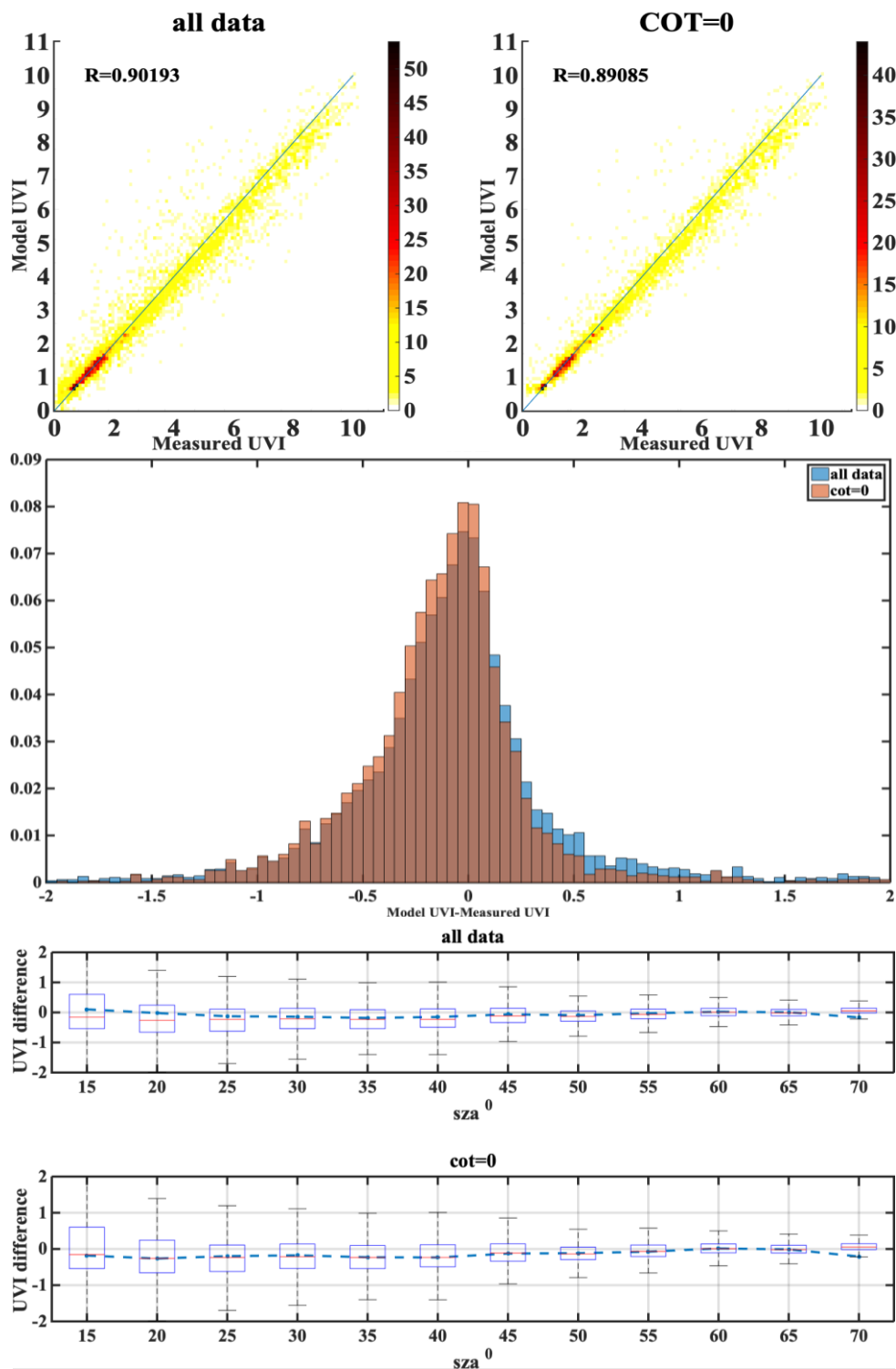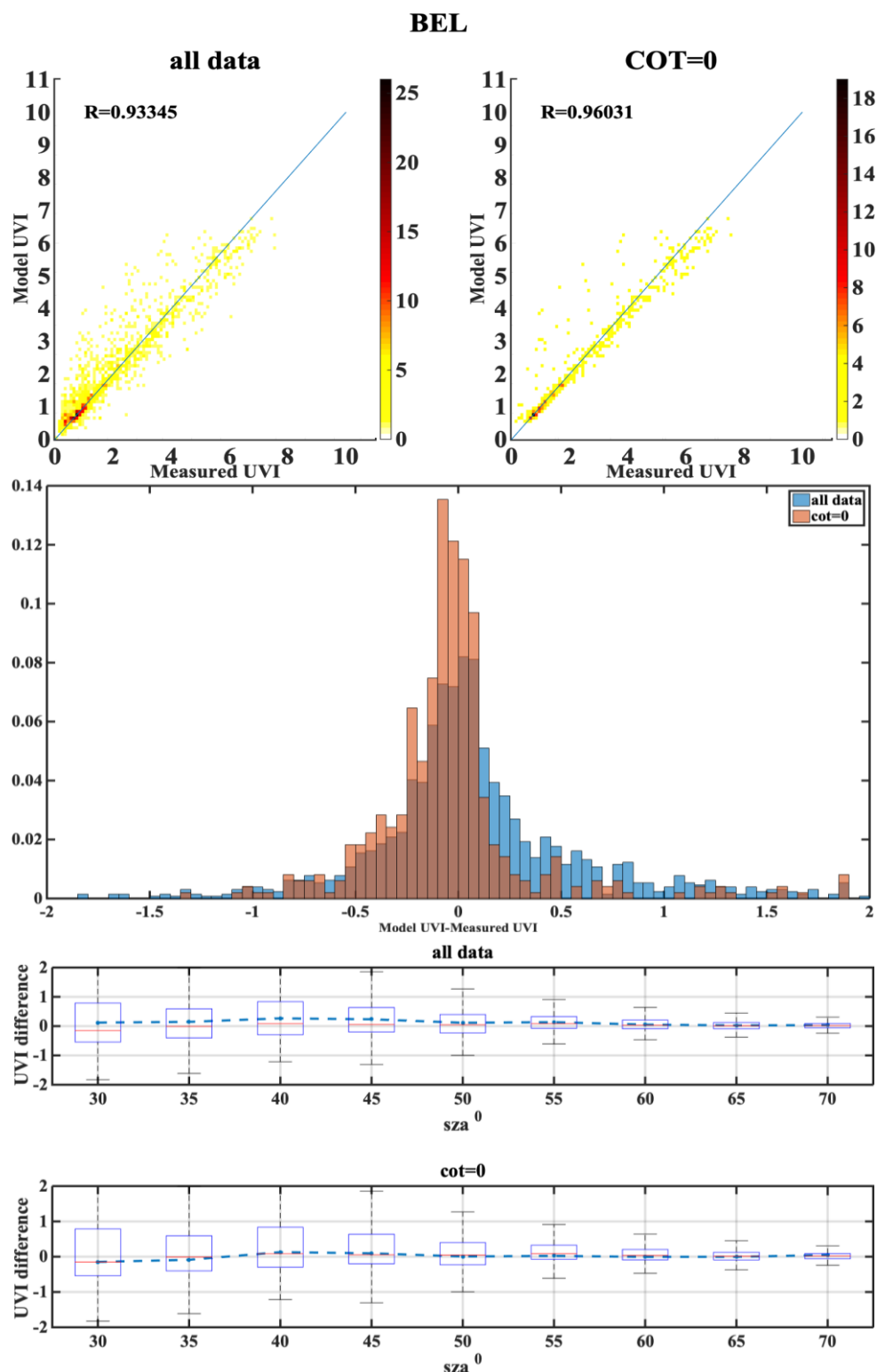
Figure A.4

Figure A.5
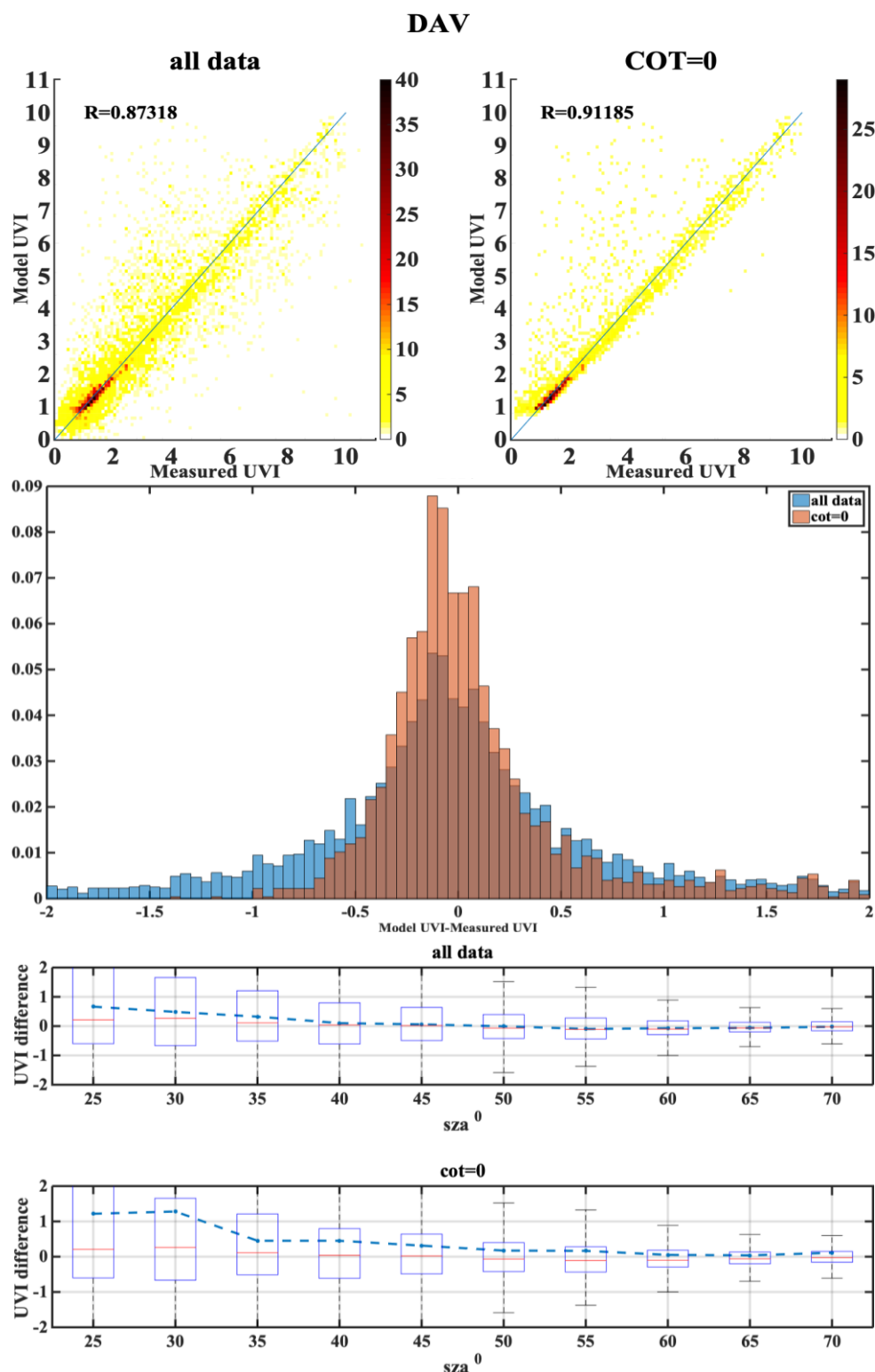
Figure A.6
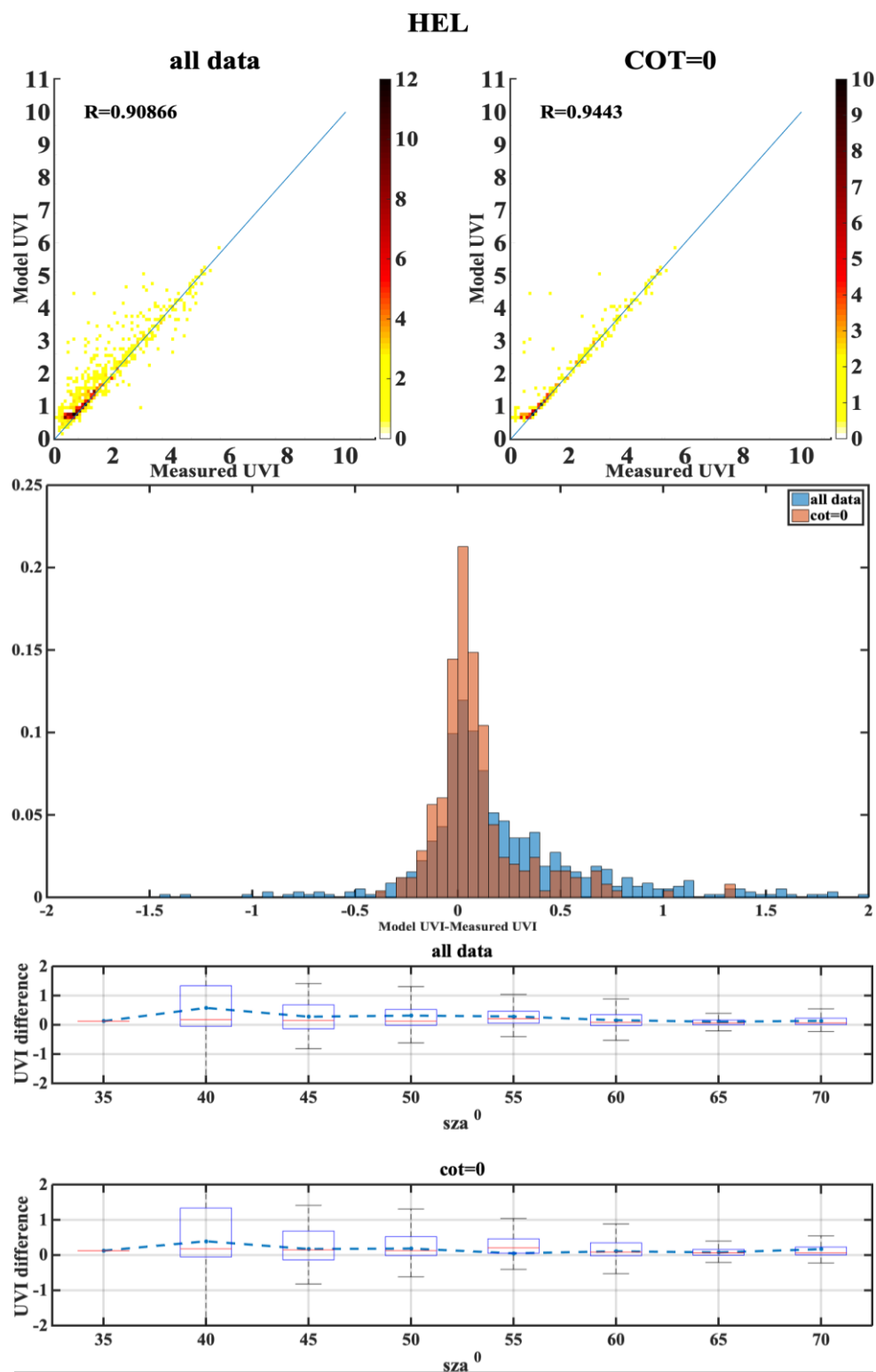
Figure A.7
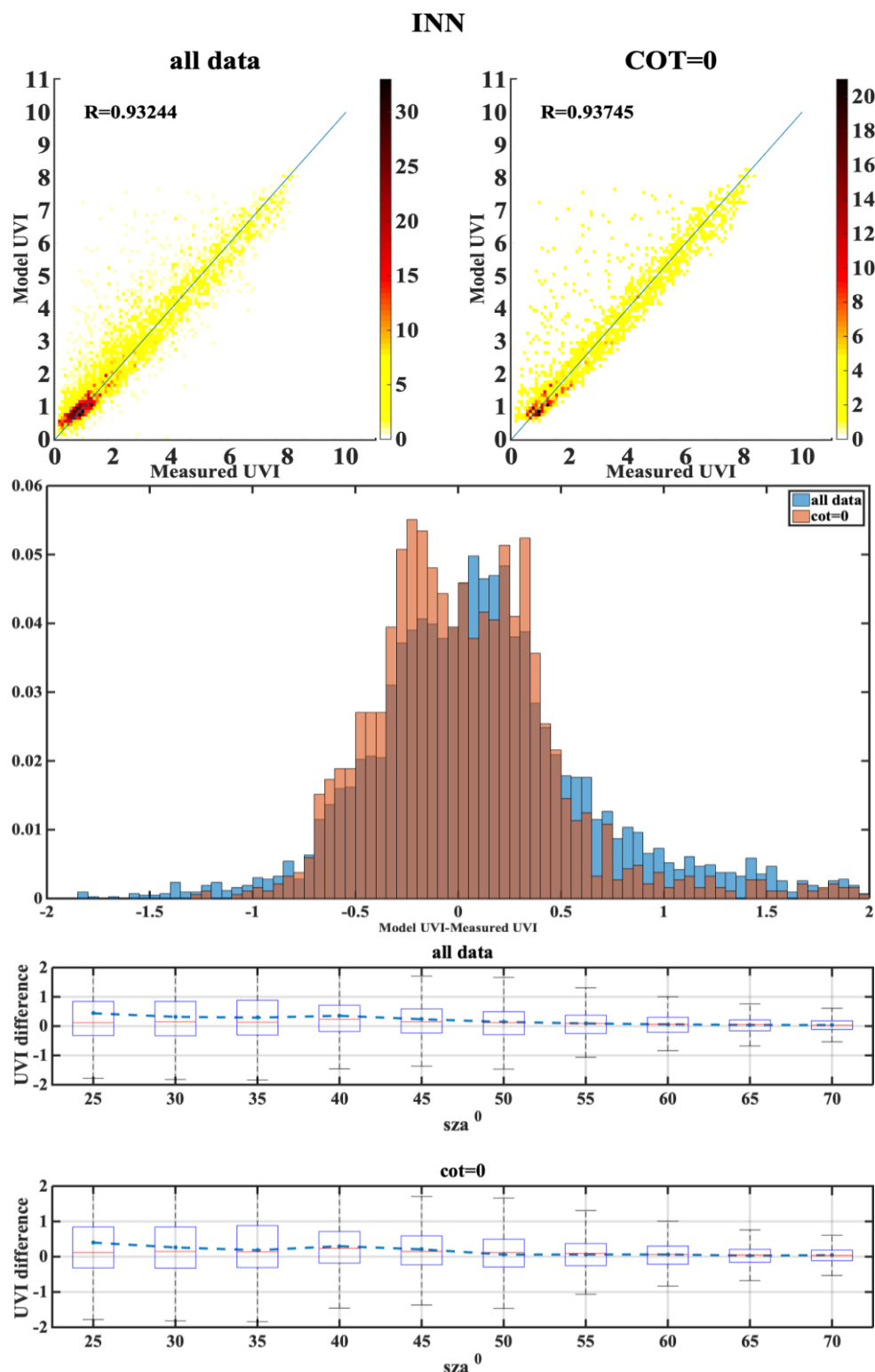
Figure A.8
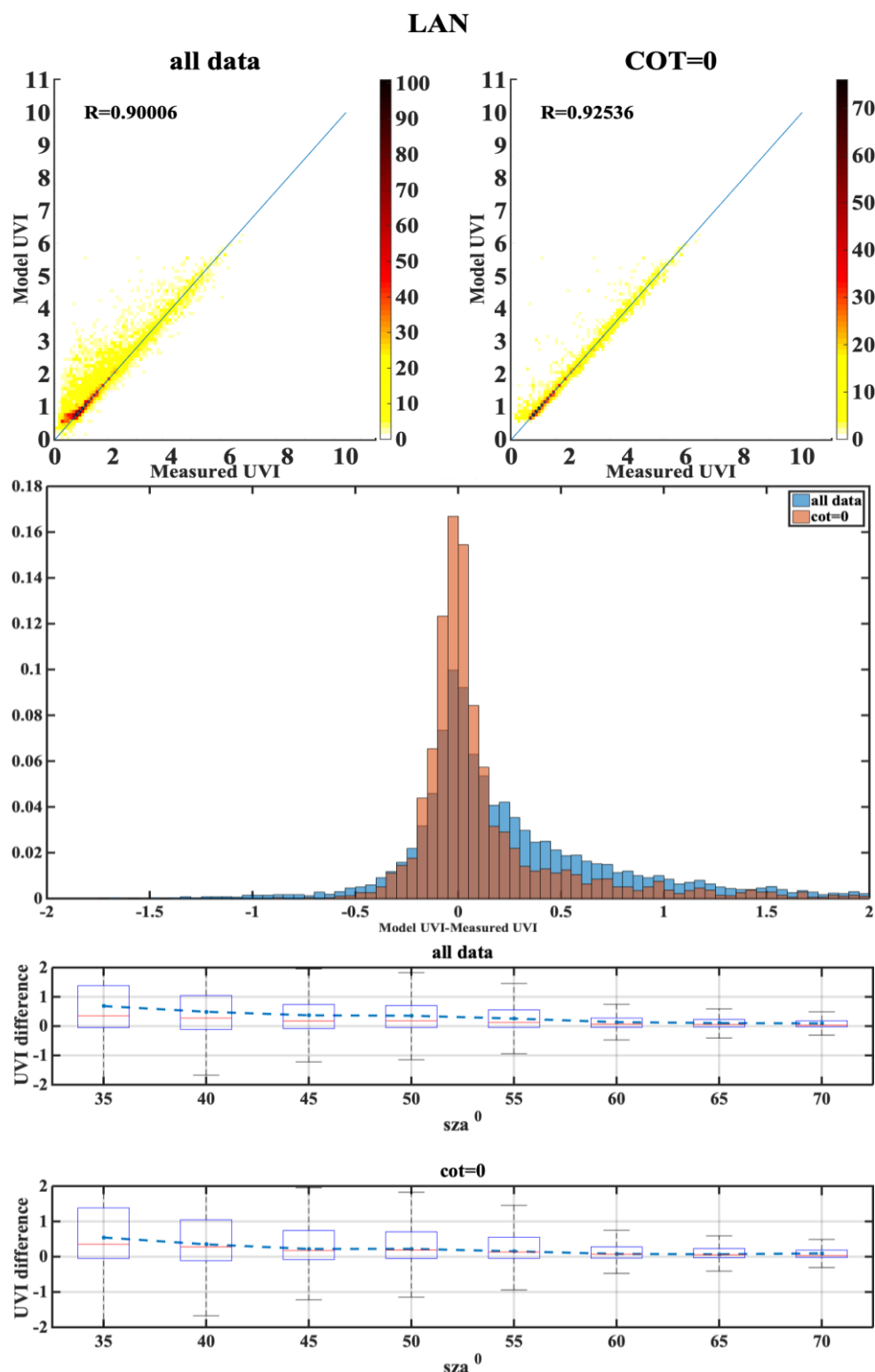
Figure A.9
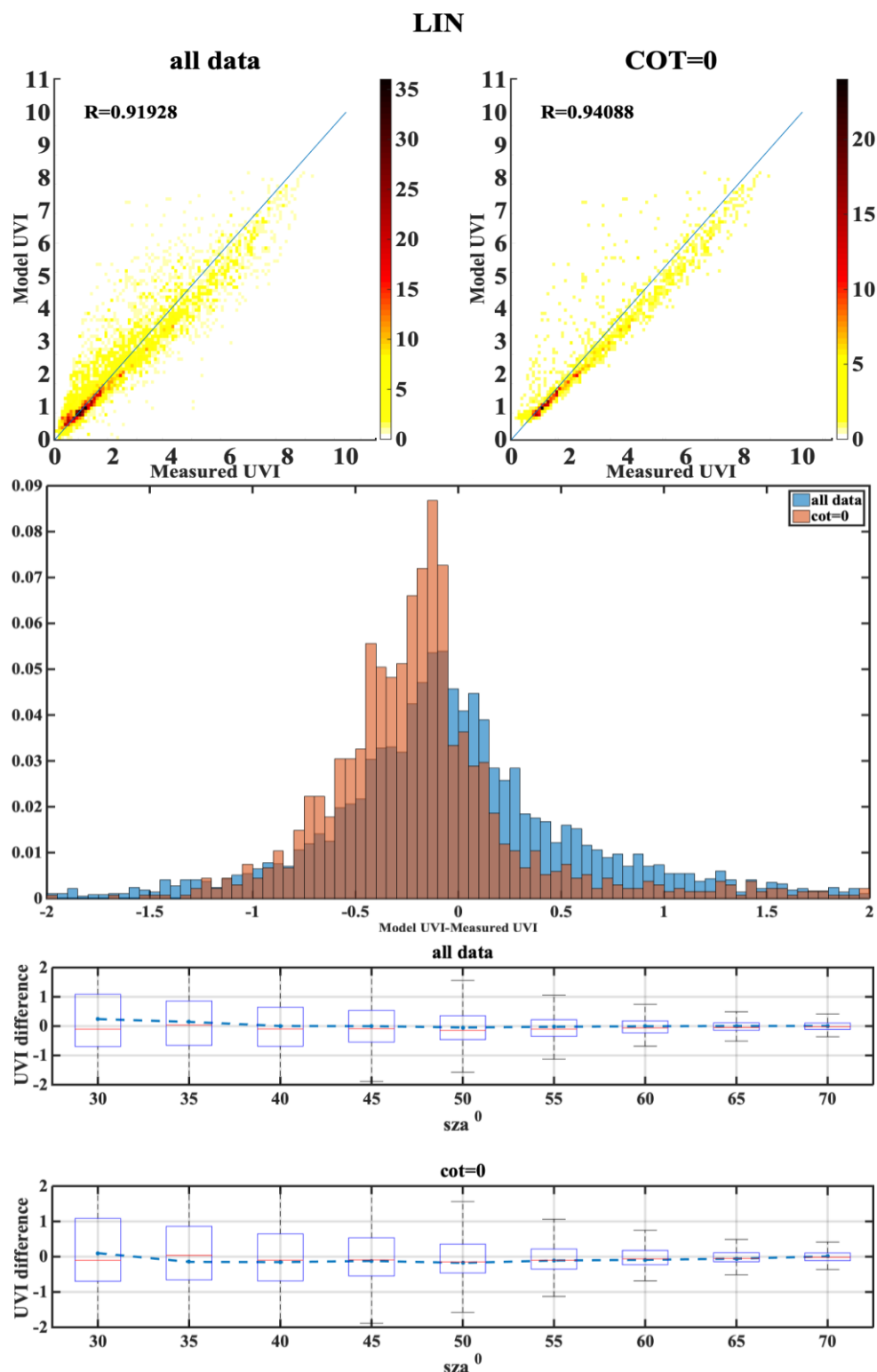
Figure A.10
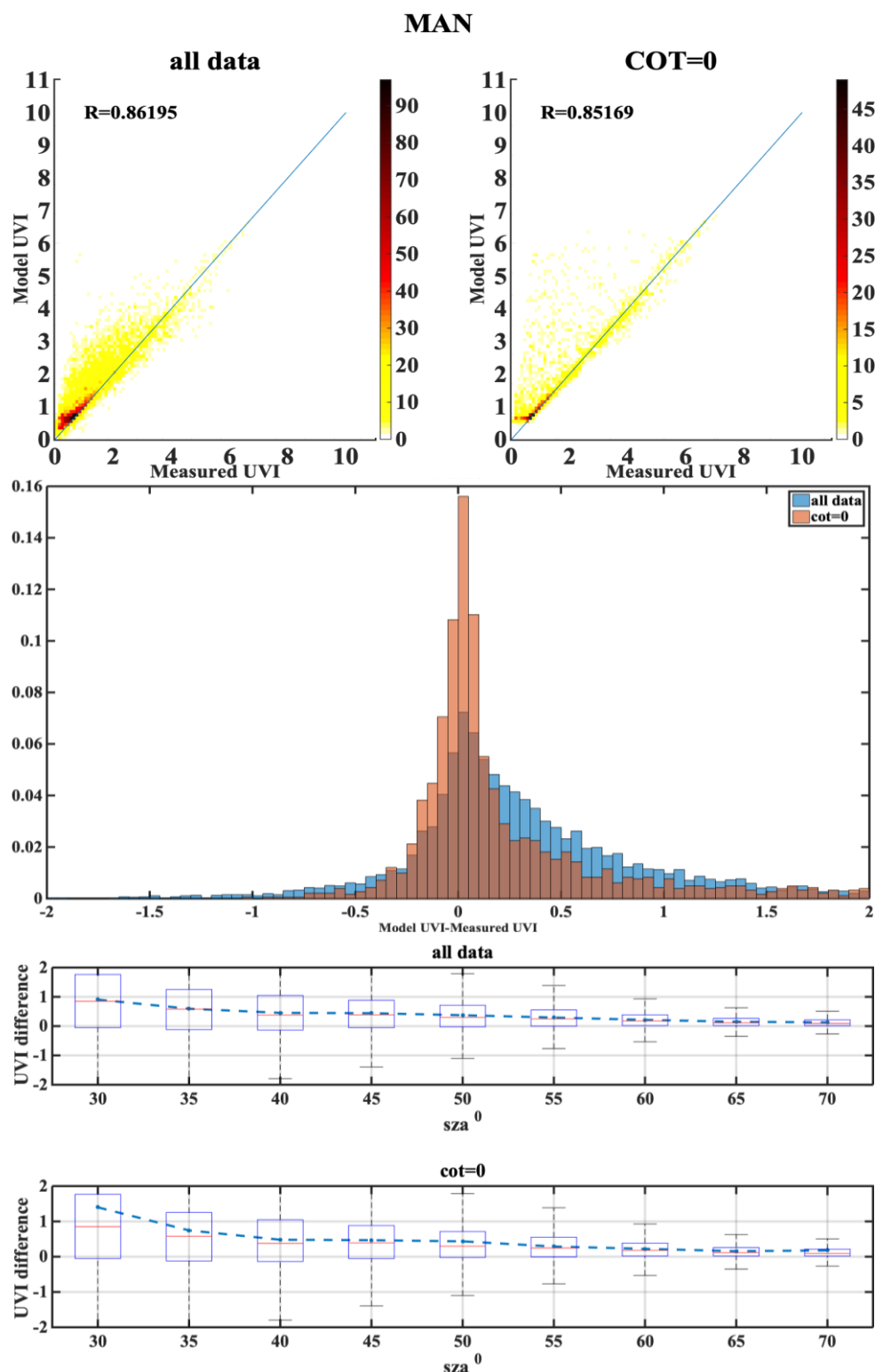
Figure A.11
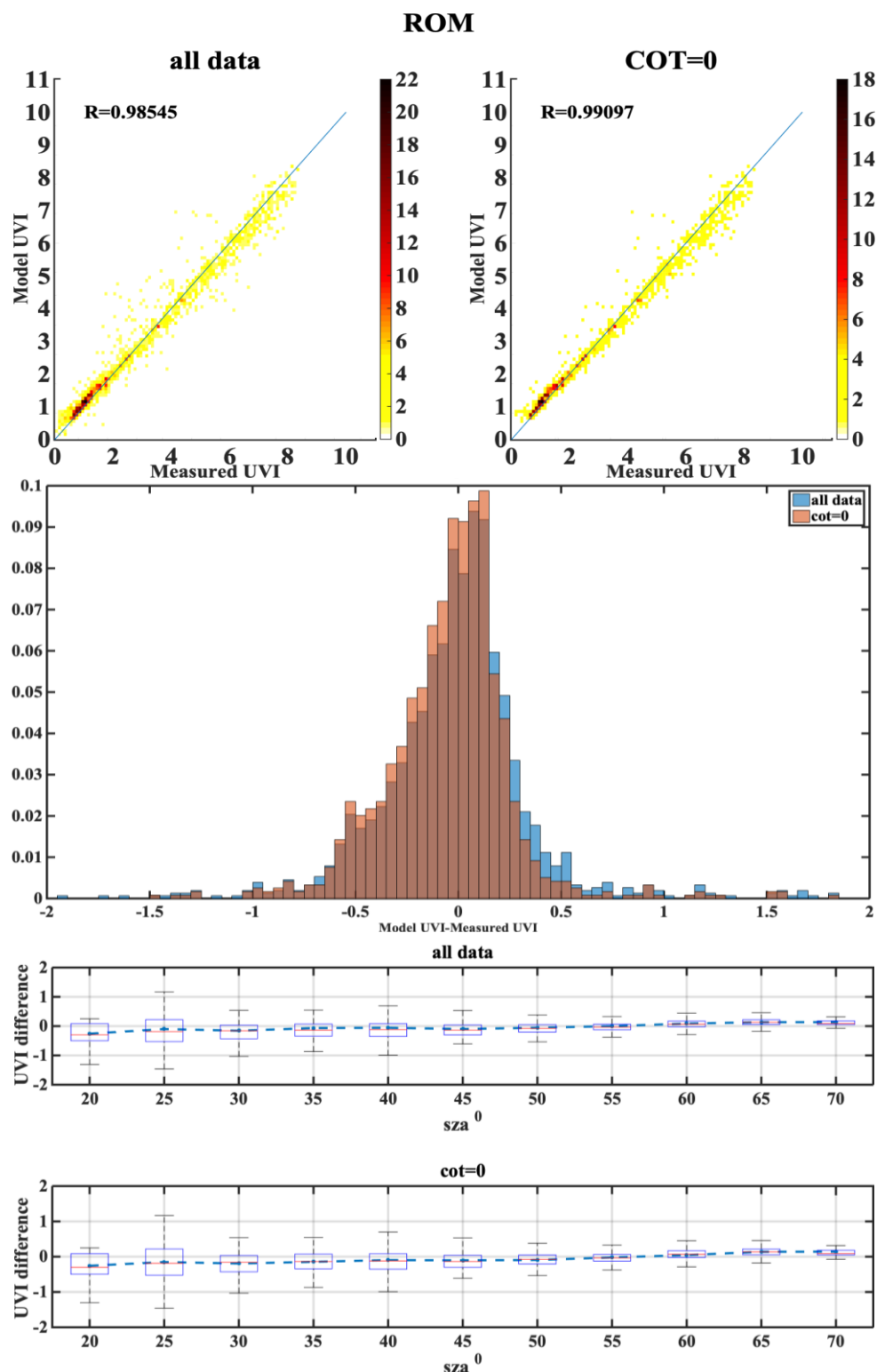
Figure A.12
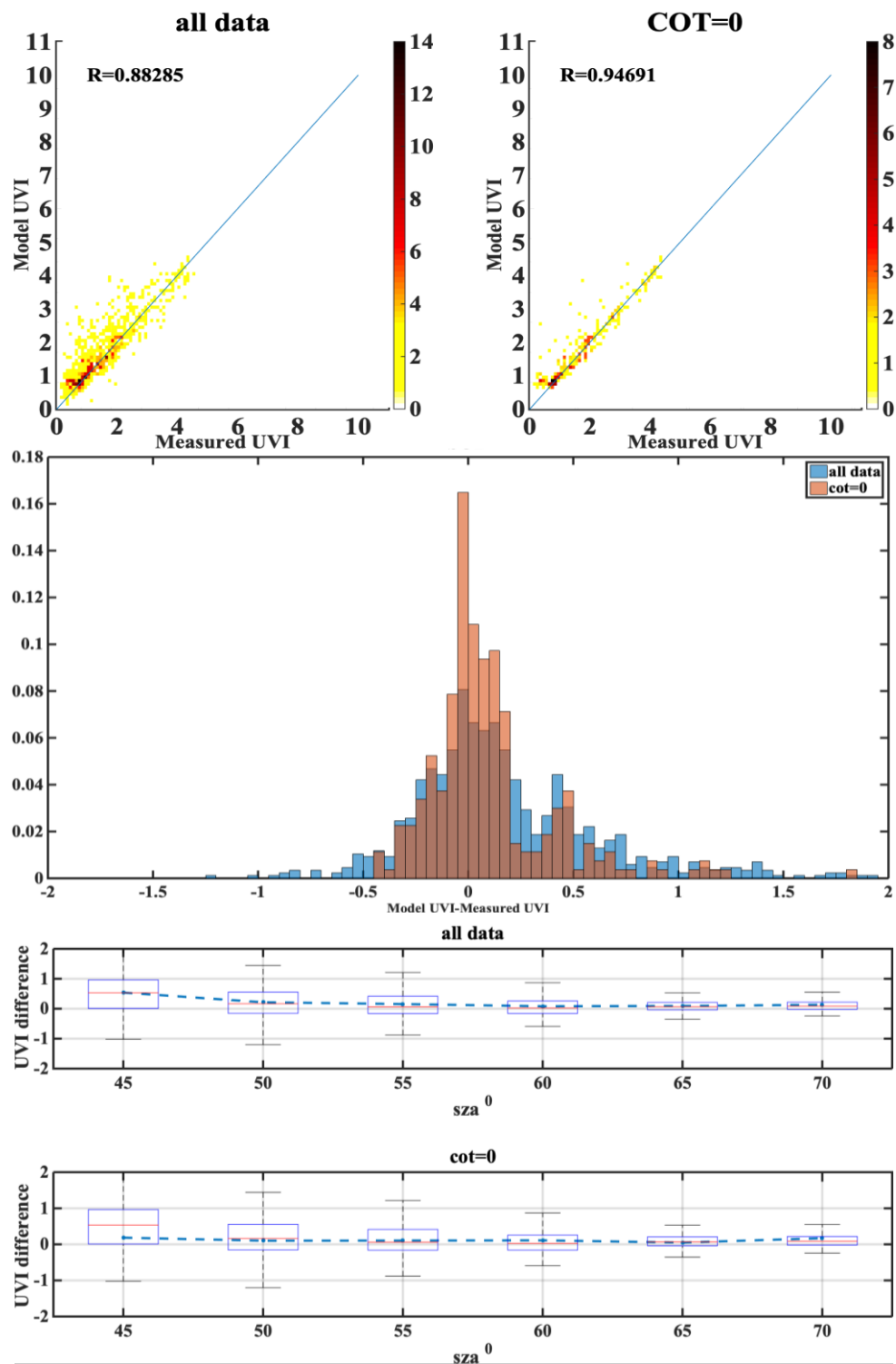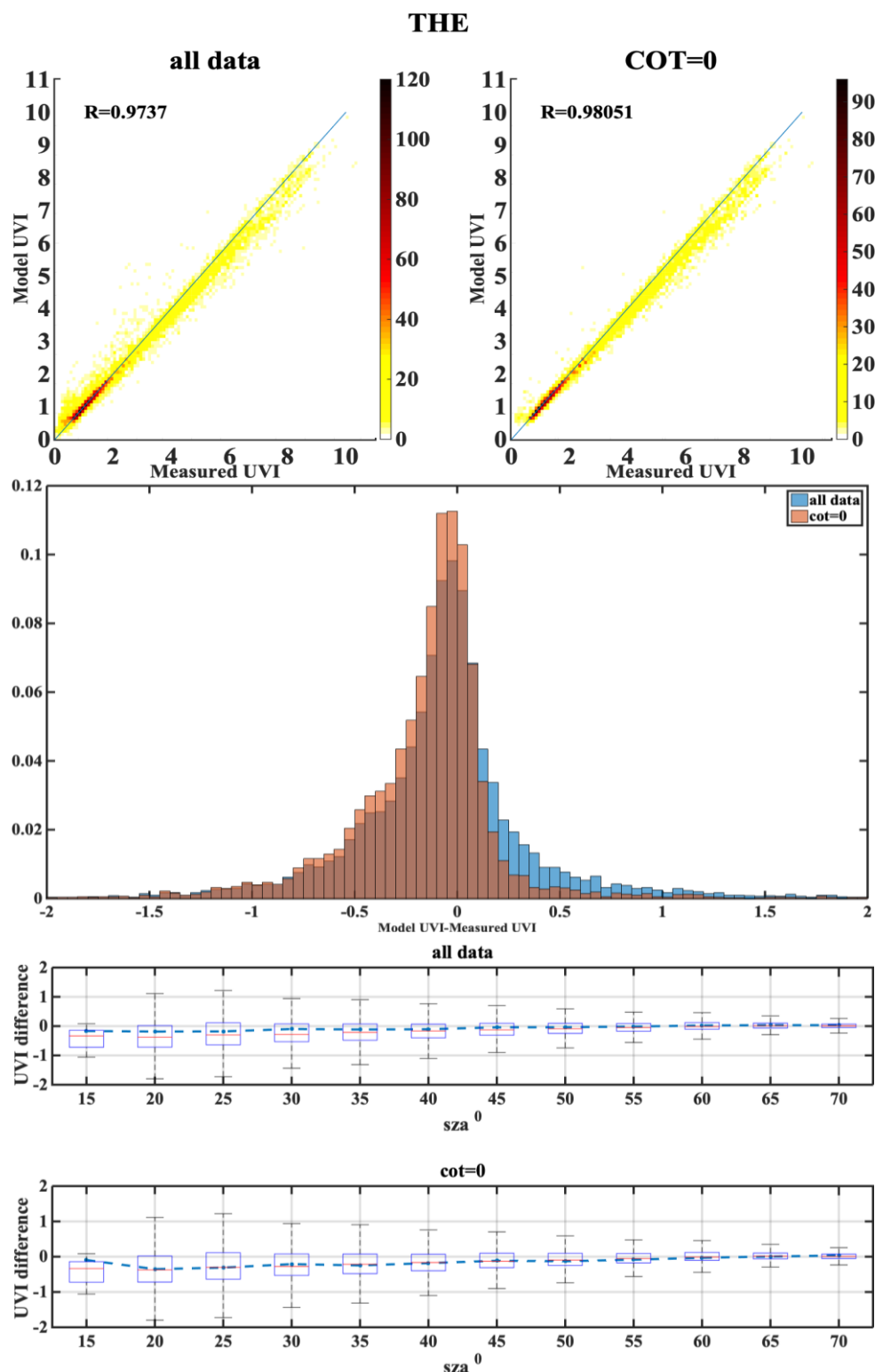
Figure A.13

Figure A.14

Figure A.15

Figure A.16

VIE

Figure A.17